Università degli Studi di Pavia

Facoltà di Ingegneria

Corso di Laurea Specialistica in Ingegneria Biomedica

Dipartimento di Meccanica Strutturale

Fracture and crack propagation study of a Superficial Femoral Artery Nitinol stent

Studio della frattura e della propagazione di una cricca in uno stent in Nitinol per l'arteria femorale superficiale

Supervisors:

Prof. Ferdinando Auricchio

Eng. Michele Conti

Author:

Marilena Santillo

Academic Year 2007/2008

Abstract

Cardiovascular disease (CVD), often related to *atherosclerosis*, is the main cause of death in Europe with over 4.35 million deaths (accounting for 49% of all deaths in 2005) resulting also in a huge economic cost: 169 billion Euro including costs to treat CVD, costs of informal care and costs due to lost productivity [1]. The third most important aterosclerotic disease, after coronary heart disease (CHD) and cerebrovascular disease, is peripheral arterial disease (PAD) of the lower limbs; among these there is the superficial femoral artery (SFA) [2]. There are several ways to treat the SFA disease but, thanks to the biomechanical features of its material, self-expanding Nitinol stent seems to be the most suitable choice. Its use, however, continues to be controversial as many of nitinol stents implanted in the superficial femoral artery (SFA) are fractured, probably because of the complex SFA's anatomy and the biomechanical forces exerted on the vessel through standing and walking, [43, 44], or because of a possible fabrication defect that can be damage it, over time.

Aim of this work is to study by a finite element commercial software (ABAQUS 6.8) how a pre-existing crack could propagate in a self-expanding Nitinol stent for the SFA. We'll simulate so how a stent behaves if it has a crack, starting from the manufacturing process and ending with the application of systolic and diastolic pressure on the vessel within which the stent will be inserted.

After an introduction to the CVD, PAD and their possible medical treatments, we'll describe: i) the anatomy and the biomechanical forces of the SFA; ii) Nitinol main features and iii) crack propagation theory. Then, we'll present a possible characterization of a crack with ABAQUS, an identification of a critical region of the stent where a crack probably arire, its collocation in this region and an analysis of the results obtained by the simulations.

Sommario

Le malattie cardiovascolari (CVD), spesso collegate all'aterosclerosi, sono la causa di morte principale in Europa con più di 4.35 milioni di morti (su 49% di morti totali nel 2005), con la conseguenza di enormi costi economici: 169 bilioni di euro, inclusi i costi per i trattamenti, per l'assistenza informale e quelli dovuti alla perdita di produttività [1]. Il terzo tipo di aterosclerosi più importante, dopo le malattie del cuore (CHD) e quelle cerebrovascolari, deriva dalla malattia delle arterie periferiche (PAD) degli arti inferiori; fra queste l'arteria femorale superficiale (SFA) [2]. Esistono diversi modi per trattare la malattia della SFA ma, grazie alle caratteristiche biomeccaniche del suo materiale, uno stent autoespandibile in Nitinol sembra essere la scelta più adatta. L'uso di questi dispositivi, tuttavia, rimane discutibile poichè alcuni degli stent in nitinol impiantati nella SFA si sono rotti, probabilmente a causa o della complessa anatomia dell' arteria e delle forze biomeccaniche esercitate sul vaso attraverso lo stare in piedi e il camminare, [43, 44], o per la presenza di un possibile difetto di fabbricazione, il quale, col passare del tempo, può danneggiare il dispositivo.

Lo scopo di questo lavoro è studiare tramite un software commerciale agli elementi finiti (ABAQUS 6.8) come una cricca pre-esistente può propagarsi in uno stent autoespandibile in Nitinol per il trattamento della SFA. Simuleremo quindi come si comporta lo stent in presenza di una cricca, a partire dal processo di fabbricazione fino all'applicazione della pressione sistolica e diastolica sul vaso all'interno del quale sarà inserito lo stent. Dopo un' introduzione sulla CVD, la PAD e i possibili trattamenti medici, descriveremo: i)l'anatomia e le forze biomeccaniche della SFA; ii) le proprietà fondamentali del Nitinol e iii) la teoria di propagazione della cricca. Presenteremo poi una possibile caratterizzazione di una cricca con ABAQUS, l'identificazione di una regione critica dello stent, cioè di una regione dove potrebbe presentarsi la cricca, la sua collocazione e i risultati ottenuti.

Acknowledgements

I would like to thank Prof. Ferdinando Auricchio to give me the opportunity to develop this thesis and gratefully acknowledge Eng. Michele Conti, PhD student, for his essential help, assistance and specially moral support. Another aknowledgement is for every single people of the Biomechanical Laboratory for their pleasantess; thantks so to Eleonora, Chiara, Giuseppe, Carla, Laura e Simone.

I'm successfull!

Bye bye

Contents

Part I

Literature & Theoretical Foundations

Chapter 1

Peripheral Artery Disease: introduction and medical treatments

The aim of the work is to study when a crack could propagate in a self-expanding Nitinol stent for the superficial femoral artery (SFA) affected by peripheral arterial disease (PAD). In this chapter, in particular, the PAD, a cardiovascular disease (CVD), is described, highlighting its risk factors, its relation with atherosclerosis and its possible treatments.

1.1 CVD and PAD

Diseases of the heart and circulatory system (cardiovascular disease - CVD) are the main cause of death in Europe. Each year CVD causes over 4.35 million deaths in Europe (accounting for 49% of all deaths in 2005). Such impact on the health of the European citizens results also in a huge economic cost. Total costs amount to 169 billion Euro including costs to treat CVD, costs of informal care and costs due to lost productivity [3, 4].

CVD is a disease that can involve heart, brain, and peripheral arteries. In Fig. 1.1 we can see the major cardiovascular events and the relative incidences.

Compared with other cardiovascular disease, it seems that PAD is the most relatively

unimportant even if, in reality, for every 100 patients with intermittent claudication (IC)[1] there are 200 of them with asymptomatic or untreated PAD [3, 6].

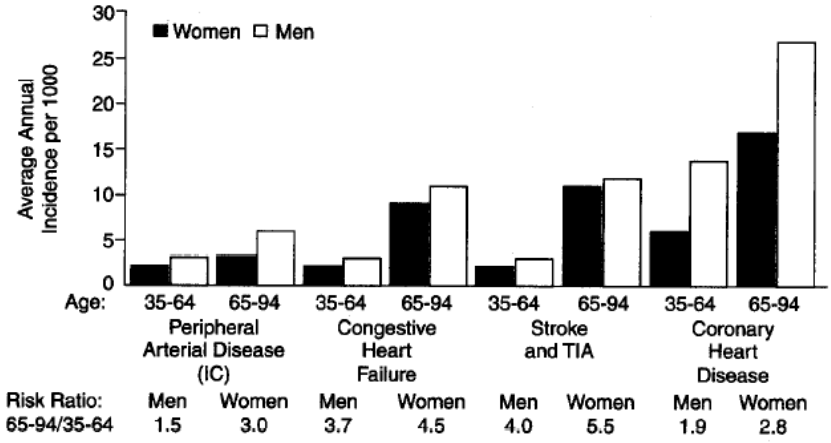

Fig. 1.1: Incidence of major cardiovascular events, Framingham Heart Study, 36-year follow-up. IC = intermittent claudication; TIA = transient ischemic attack [5].

In general, peripheral arterial disease comprises those entities that result in arterial occlusion of vessels other than those of the coronary and intracranial vascular beds. Although the definition of PAD technically includes problems within the extracranial carotid circulation, the upper extremity arteries, and the mesenteric[2] and renal circulation, it's often mainly associated to the chronic arterial occlusive disease in the legs arteries. Hence, when we'll talk about PAD we'll talk principally about a leg artery disease.

IC is the earliest and the most frequent presenting symptom in patients with lower extremity PAD [7], and it is correlate to a number of risk factors.

Epidemiological data show that among them there are male gender, aging, family history, smoking, diabetes, hypertension, dyslipidaemia and hyperhomocysteinemia [7].

Fig. 1.2 summarizes graphically the approximate influence or association between some of the above factors and PAD, taking a global view of the existing evidence.

If not controlled, these risk factors may lead to the obstruction of the lower limb arteries,

[1] **IC:** pain in the muscles of the leg with ambulation.

[2] **Mesenteric circulation:** circulation of blood through the vessels supplying the abdominal viscera.

an important manifestation of atherosclerosis that is defined as an inflammatory vascular pathology in which a plaque, made up of fat, cholesterol, calcium, and other substances founded in the blood, builds up on the insides of arteries (Fig. 1.3) and over time, hardens and narrows them [8].

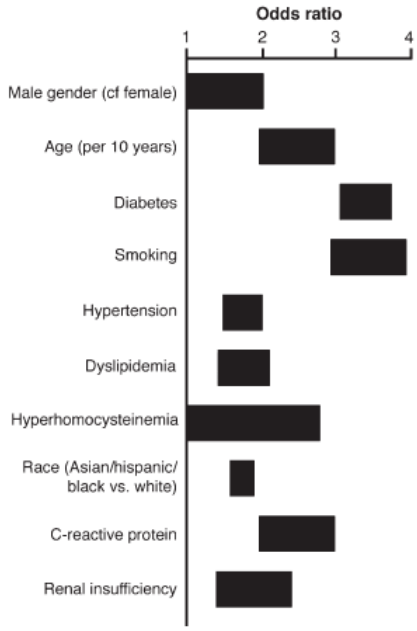

Fig. 1.2: Approximate range of odds ratios for risk factors for symptomatic peripheral arterial disease [7].

Patients with intermittent claudication have normal blood flow at rest and therefore no limb symptoms but, with exercise, occlusive lesions in the arterial supply of the leg muscles limit the increase in blood flow, resulting in a mismatch between oxygen supply and muscle metabolic demand that is associated with the symptom of claudication [7].
As the disease progresses in severity, patients might have pain at rest, too. In the late stages of PAD, tissue hypoperfusion progresses to ischaemic ulceration and gangrene, and major amputation is eventually required in more than a third of these patients [9].
Mortality is closely linked with the presence of rest pain or tissue loss, the so called critical limb ischaemia (CLI), with a 1-year mortality rate of about 20% in several series [10, 11].

For all these reasons it became very important to treat the PAD when it is not yet advanced. Sometimes, a change in the style of life it's enough to treat atherosclerosis but when the disease becomes more serious it will be necessary looking for medical procedures

and surgery (bypass, angioplasty or stenting).

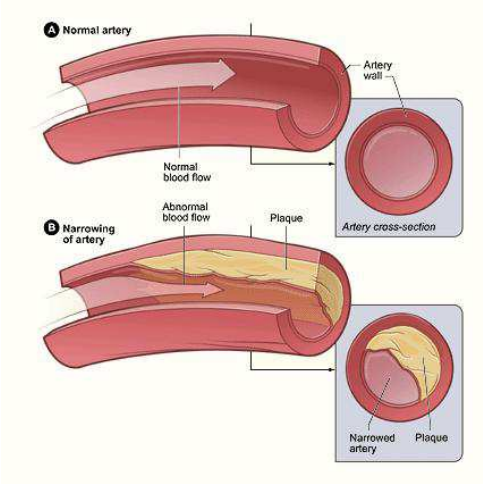

Fig. 1.3: Normal artery with normal blood flow and with a plaque buildup.

1.2 PAD medical treatment

The management of patients with lower extremity PAD is two-pronged, addressing firstly the risk factors of generalized atherosclerosis in importance progression, and then acting with treatments such as *pharmacotherapy*, *endovascular therapy*, or *surgery* to treat the lower extremity symptoms [12].

In Fig. 1.4 we can see the stages of PAD treatment starting from the intermittent claudication phase and ending, if necessary, with stent placement.

Obviously, the treatment should be chosen on the basis of the severity of the symptoms severity.

Invasive intervention for symptomless disease is never appropriate even if the presence of this symptomless disease often should be used as a marker of generalized atherosclerosis. Similarly, patients with mild or moderate claudication symptoms are best treated with conservative measures such as the institution of an exercise programme [12].

Pharmacotherapy is usually used as an adjunctive treatment to improve walking, although no agent has provided sufficient efficacy to gain widespread acceptance and for patients

with chronic limb-threating ischaemia it can be considered when, for any reasons, a surgical revascularisation procedure is impossible.

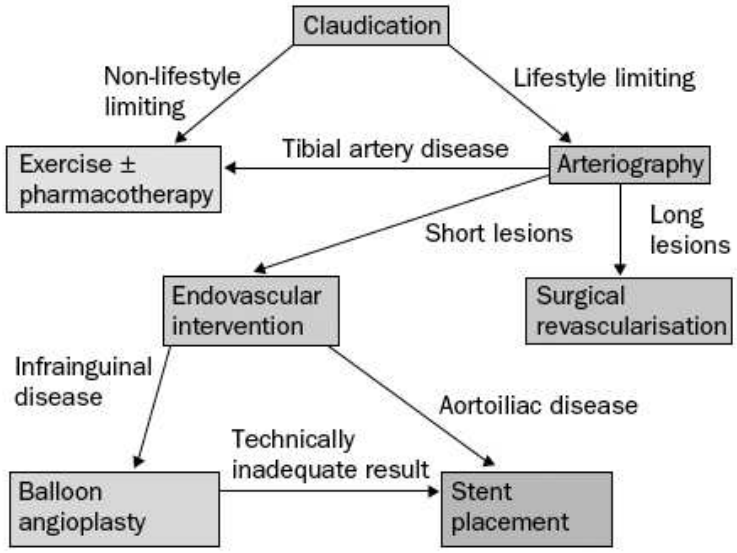

Fig. 1.4: Algorithm for managing a patient with intermittent claudication [12].

Surgical revascularisation, instead, is unquestioned as appropriate therapy for patients with chronic critical limb ischaemia, directed at the prevention of limb-loss and its accompanying disability.

By contrast, surgical intervention is rarely indicated in patients with intermittent claudication alone, since the risk of major amputation is exceedingly low. Only in patients whose symptoms interfere with their lifestyle or with the performance of an occupation, the benefits of surgical revascularisation will outweigh the risks.

The possible basic treatments when surgery is chosen are [13]:

1. endarterectomy, an acceptable option when there is a truly localized disease that causes the narrowing of the aorta and common iliac arteries alone, for example, as it wants to remove the atheromatous plaque material, or blockage, in the lining of the constricted artery.

2. bypass grafting, used in the other cases when patency rates are unsatisfactory.

Endovascular catheter interventions to treat occlusive lesions of the lower extremities, first described by Dotter and Judkins in 1964 [16], are attractive alternatives to open surgical procedures such as bypass and endarterectomy.

In the following sections, therefore, we'll introduce the two most important of them (angioplasty and stenting) even if focusing, obviously, on the type of our interest: the stenting.

1.2.1 Angioplasty

Angioplasty is a percutaneous technique used to dilate an area of arterial blockage with the help of a catheter that has an inflatable small sausage-shaped balloon at its tip and is introduced in the groin (or sometimes the arm) through a little needle hole, and then placed within a blood vessel. Compared with bypass surgery, it is much less invasive and can be repeated if the patient develops disease in the same or another artery in the future. In Fig. 1.5 we can see the difference between a channel of a normal, reduced and treated artery and in Fig. 1.6 we can also see the angioplasty procedure: a catheter with a guidewire is placed in the femoral artery of the leg, a dye is then injected, in order to visualize shadows of the inner artery lumen and, when a narrowed segment is identified, the balloon-tipped catheter is passed and inflated into this area. The balloon compresses the plaque that is causing the narrowed area and squashes it outwardly against the arterial walls.

(a) (b) (c)

Fig. 1.5: Atherosclerotic vessel. a)Rounded unobstructed channel of a normal coronary artery (cross-sectional view); b)the channel (through which blood flows) is significantly reduced by a blockage and c) an increased opening after the blockage was dilated or opened up with balloon angioplasty.

Many angioplasty procedures also include the placement of a stent. Therefore, we'll describe what is a stent showing even the differences between a self-expanding and a balloon-

expanding one.

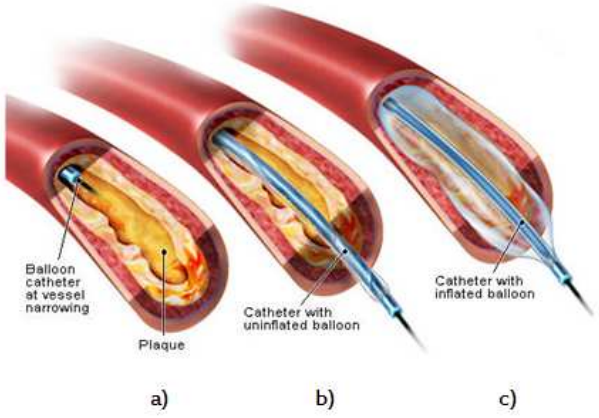

Fig. 1.6: Scheme of a balloon angioplasty procedure a) Balloon insertion; b) Balloon inflation; c) Balloon deflation.

1.2.2 Stenting

A stent is typically designed as a tubular support structure implanted within an artery or another vessel and then expanded from a compressed diameter to an expanding one.
Once the stent is positioned and expanded into the vessel to be treat, the tubular support structure of the stent contacts and radially sustains the inner wall of passageway, thereby preventing it from closing.

Stents are generally classified as

- balloon-expanding (BX)
- self-expanding (SX)

depending upon how the deployment is done. Both devices, however, have clearly the same goal even if a very different mechanical behavior.
BX stents are manufactured in the crimped state and expanded the vessel diameter by inflating a balloon, thus plastically deforming the stent.
SX stents instead are manufactured at the vessel diameter (or slightly above) and crimped

and constrained to a smaller diameter until the intended delivery site is reached. The constraint is then removed and the stent deployed. Accordingly, BX stents resist the balloon expansion process, whereas SX stents assist vessel expansion [17].

Balloon-expanding stents

As previously said, the expansion of BX stent is achieved by the balloon inflation which provides plastic deformation of the stent. In particular the procedure provides that the BX is mounted on a folded angioplasty balloon and expanded to the desired diameter by inflation of the balloon. Subsequently, the balloon is deflated and removed, leaving the stent at the targeted site (Fig. 1.7).

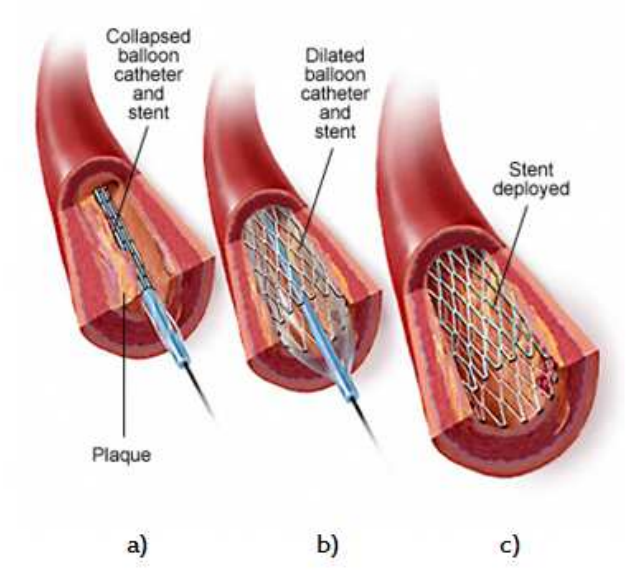

Fig. 1.7: Scheme of a balloon expanding stent procedure. a) Stent insertion; b) Balloon inflation; c) Expanded stent.

BX stents can be classified into two groups:

- *coil design*;
- *tube design*.

Coil design stents (Fig. 1.8a) incorporate a continuous wound wire or a series of flat sheet coils, have a large strut width, a gap and no connections between struts providing them high flexibility. However, the design lacks radial strength, and the wide gap allows tissue damage since the tissue prolapses between the wire elements.
Tube design stents are cut from a steel tube, or obtained from a metal sheet which is rolled and welded [18].
Both stents anyway, after the introduction, have been the topic of many clinical studies in the years.

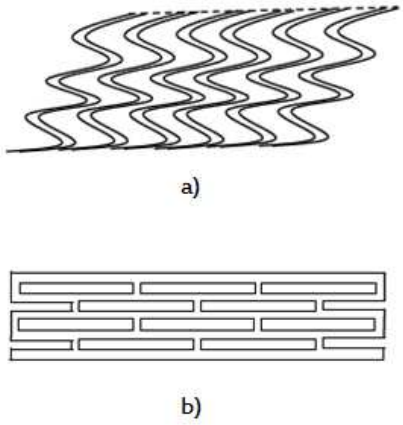

Fig. 1.8: a) Coil and b) tube design.

Self-expanding stents

Self-expanding stents do not require a balloon and they are manufactured with a diameter larger than that of the target vessel, crimped and restrained in a delivery system and finally elastically released into the target vessel.

Many different types of SX stent designs are available in the market and they can be classified as:

- wire-based stent (Fig. 1.9a), made of stainless steel woven monofilaments ;
- sheet-based stent (Fig. 1.9b), based on the idea to roll a sheet, previously laser-cut, and weld or fix it at specific struts [20];
- tube-based stent (Fig. 1.9c).

Performance of SX stents, however, is limited by the ability of the material to store elastic energy while constrained in the delivery system and consequently superelastic stents become a more suitable choice [21].

Superelastic SX stents

Superelasticity refers to the ability of Nitinol and certain other metals to return to their original shape after severe deformations. As such, it is an extension of the conventional elasticity that all metals exhibit to varying degrees: stainless steel (SS) can return to its original length if stretched up to 0.3% of its original length, extremely elastic titanium alloys up to 2%, and superelastic Nitinol, over 10%. Superelastic materials, macroscopically, appear to be simply very elastic but, practically, the mechanism of their deformation is quite different from conventional elasticity. For example, when a stress is applied to Nitinol, and after a rather modest elastic deformation, superelastic Nitinol changes its crystal structure from austenite to martensite where:

- austenite, or parent crystal structure, is cubic;
- martensite, or daughter structure, is complex monoclinic.

This "stress assisted" phase transition allows the material to change shape as a direct response to the applied stress and when the stresses are removed, the material reverts to the original austenite and recovers its original shape. It's important to note that the narrow temperature range within which Nitinols superelasticity is exhibited includes body temperature, yielding this alloy material of choice for designers of SX stents.

Numerous vessels throughout the vascular system may benefit from treatment by a stent. Among them there is also the SFA.

In the next chapter, therefore, we will introduce it, focusing more attention on the nitinol stent use and on the possible reasons of its fracture.

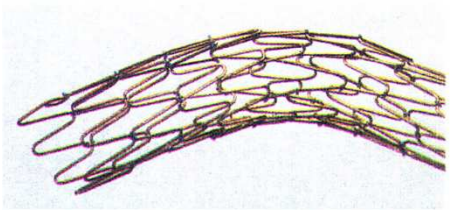

(a)

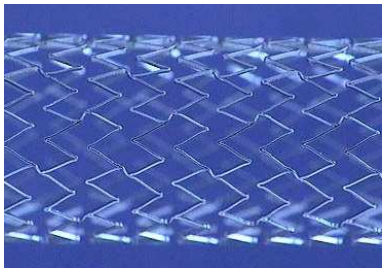

(b)

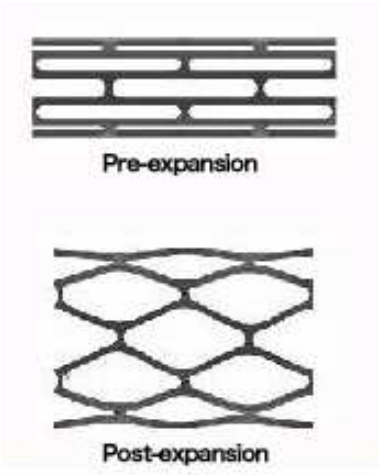

(c)

Fig. 1.9: Design examples of a) wire-stent , b) sheet-stent and c) tube-stent.

Chapter 2

SFA disease: overview and treatments

As we discussed in the previous chapter, PAD is often mainly associated to the chronic arterial occlusive disease in legs arteries. In this chapter we will discuss the SFA disease and its possible treatments, focusing on nitinol stenting and to the main possible causes of its fracture.

2.1 Introduction

Percutaneous interventional treatments for SFA disease have long suffered from excessively high restenosis[1] rates regardless of treatment with PTA (Percutaneous Transluminal Angioplasty) alone or with stenting [24].
Stent implantation seems to be the most popular approach to date as it reduces vessel recoil and remodeling, two of the main contributing factors in restenosis. However, the neointimal hyperplasia, (Fig. 2.1), the most important mechanism of restenosis, remains a significant problem [26].

[1] **Restenosis:** name given to the formation of new blockages within an artery, after it has been treated with angioplasty or stenting.

In coronary arteries, stents that deliver local concentrations of pharmacologic agents over a prolonged period without systemic toxicity have been developed to prevent the formation of in-stent neointimal proliferation [25, 26].
As for the SFA, there is only one study reporting a local drug delivery, the Sirolimus-Coated Cordis Self-Expandable Stent (SIROCCO) trial.
With its two versions, SIROCCO I and SIROCCO II, this trial demonstrates that there are no significant differences between a bare and a coated stent; both are safe, effective, and able to sustain patency in the SFA disease but whether these effects can be maintained beyond 6 months remain to be determined [27].

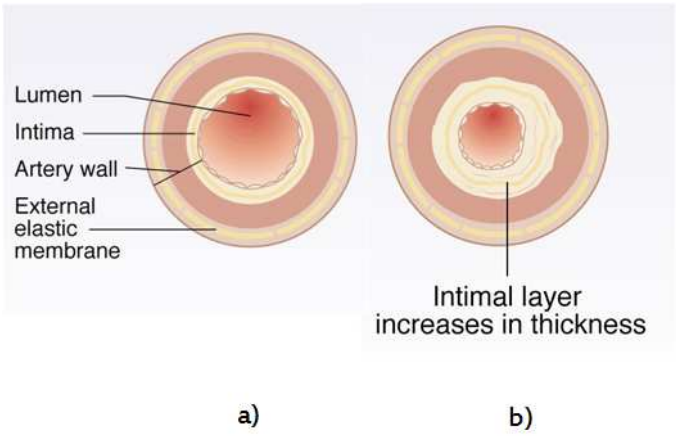

Fig. 2.1: a) Normal vessel layers. b) Vessel with neointimal hyperplasia. Note the thickness increase of the intimal layer.

Stenting, therefore, continues to be the preferred solution in SFA disease treatment.
In the following section we review the features that a stent should have in order to successfully treat occlusions in the SFA and other peripheral arteries.
these ones.

2.2 Self expanding Nitinol stent

A stent for the treatment of the SFA disease preferably:

- would be able to deform elastically (i.e., recoverably) in response to external stresses

and revert back to its original expanded shape when the stress is relieved;

- should be designed in a configuration that allows a large and uniform radial force to be exerted on the vessel wall when the stent is deployed, condition preferred to ensure that the stent, in its expanded state, compresses occlusions and holds the vessel open. Indeed, a stent that exerts a large and uniform radial force when deployed is also better able to resist external traumas.
- should be highly flexible axially both in bending and torsion to accommodate the stresses that are experienced by the implanted stent as a result of body motions and the curvature inherent to body vessels ;
- should have good fatigue properties since it may be exposed to multiple external traumas while implanted. With each trauma, the stent must withstand the impact and return to its original configuration. In vessels such as the SFA, a stent is also subject to constant expansion and compression due to the pulsation of blood flow, which also must be considered in designing the fatigue behavior of a stent.
- should have a uniform circumferential stiffness to minimize the difficulties associated with compressing or crimping the stent to a reduced diameter for delivery into a vessel for treatment.

Thanks to its properties (ref. Section 3.1), Nitinol is the actual more used material adopted to realize a stent that best meets the requirements listed above [28].
More recent SFA stent reports using self-expanding nitinol designs have shown improved 1- to 2-year primary and secondary patency rates, but secondary reintervention rates for occlusion or in-stent restenosis (ISR), due to the fracture of the stent, remain high (20%-30% at 1 year) [29, 30].
The reasons for this high rate of restenosis in stented femoropopliteal arteries have not been fully elucidated. One hypothesis is that they may be a function of the unique biomechanical forces that are present in stented infrainguinal arteries [31].

In the following sections, therefore, it becomes appropriate to briefly introduce the complex anatomy of the SFA [32], and the acting biomechanical forces [31, 33, 34], two important factors both for the atherosclerosis formation and for the device failure.

2.3 SFA anatomy description

The following anatomy informations about the SFA and what surrounded it are taken from a book of H.Gray [35].

The **femoral artery** (Fig. 2.2) is described as a large artery that starts in the lower abdomen and goes down into the thigh, as a continuation of the external iliac artery which comes from the abdominal aorta. It begins immediately behind the inguinal ligament, midway between the anterior superior spine of the ilium and the symphysis pubis, passes down the front and medial side of the thigh and ends at the junction of the middle with the lower third of the thigh, where it passes through an opening in the Adductor magnus to become the popliteal artery. The vessel, at the upper part of the thigh, lies in front of the hip-joint; in the lower part of its course, it lies to the medial side of the body of the femur, and between these two parts, where it crosses the angle between the head and body, the vessel is some distance from the bone.

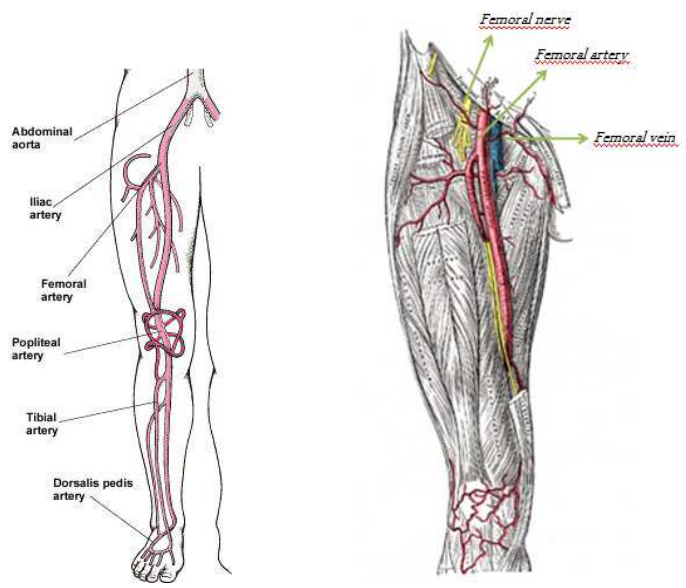

(a) (b)

Fig. 2.2: a) Femoral artery, b) vein and nerve. As it's possible to see it starts behind the inguinal ligament, passes down the front and medial side of the thigh and ends in its lower third.

The first 4 cm of the vessel is enclosed, together with the femoral vein, in a fibrous sheath called **femoral sheath** (Fig. 2.3) while in the upper third of the thigh the femoral artery is contained in the **femoral triangle**, or *Scarpa's triangle* (Fig. 2.4), and in the middle third of the thigh, in the **adductor canal** (*Hunter's canal*).

The **femoral sheath** (crural sheath) assumes the form of a short funnel, the wide end of which is directed upward, while the lower, narrow end fuses with the fascial investment of the vessels, about 4 cm below the inguinal ligament.
The lateral wall of the sheath is vertical and is perforated by the lumboinguinal nerve; the medial wall is directed obliquely downward and lateralward, and is pierced by the great saphenous vein and by some lymphatic vessels.
The sheath is divided by two vertical partitions which stretch between its anterior and posterior walls.

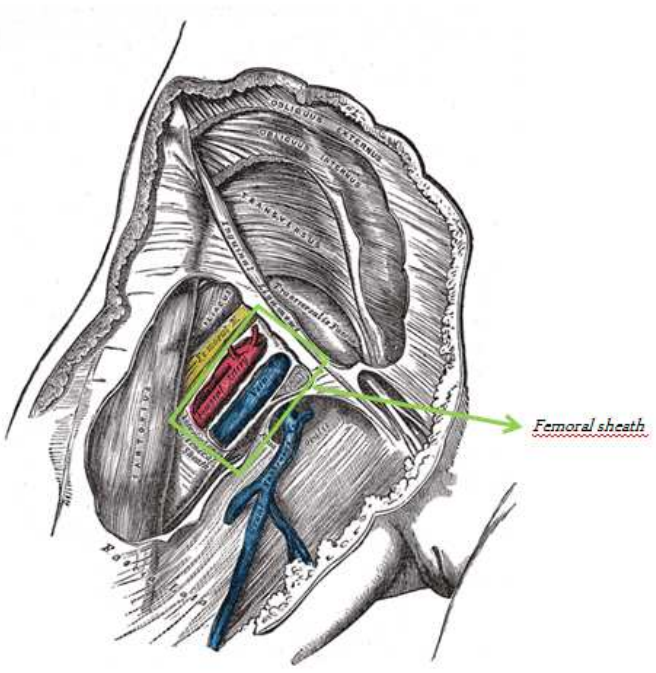

Fig. 2.3: Femoral sheath laid open to show its three compartments: the *lateral* that contains the femoral artery (in red), the *intermediate* that contains the femoral vein (in blue) and the *medial* and the smallest one, named femoral canal, that contains some lymphatic vessels.

The lateral compartment contains the femoral artery, and the intermediate the femoral vein, while the medial and smallest compartment is named **femoral canal**, and contains some lymphatic vessels and a lymph gland embedded in a small amount of areolar tissue. The femoral canal is conical and measures about 1.25 cm in length.

The **femoral triangle** (*trigonum femorale; Scarpas triangle*) corresponds to the depression seen immediately below the fold of the groin. Its apex is directed downward, and the sides are formed laterally by the medial margin of the Sartorius, medially by the medial margin of the Adductor longus, and above by the inguinal ligament.
The floor of the space is formed from its lateral to its medial side by the Iliacus, Psoas major, Pectineus, in some cases a small part of the Adductor brevis, and the Adductor longus, and it is divided into two nearly equal parts by the femoral vessels, which extend from near the middle of its base to its apex: the artery giving off in this situation its superficial and profunda branches, the vein receiving the deep femoral and great saphenous tributaries. On the lateral side of the femoral artery there is the femoral nerve divided into its branches. Besides the vessels and nerves, this space contains some fat and lymphatics.

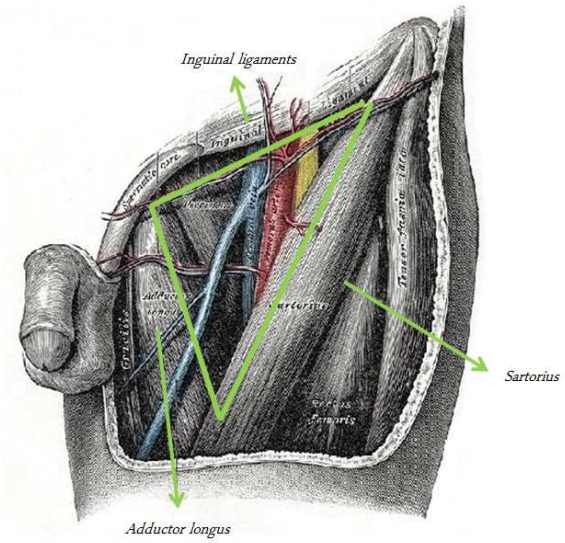

Fig. 2.4: The left femoral triangle. Laterally it was delimited by the medial margin of the Sartorium, medially by the medial margin of the Adductor longus and above by the inguinal ligament.

The **adductor canal** (*canalis adductorius; Hunters canal*) is an aponeurotic tunnel in the

middle third of the thigh, extending from the apex of the femoral triangle to the opening in the Adductor magnus. It is bounded, in front and laterally, by the Vastus medialis, behind by the Adductores longus and magnus, and is covered in by a strong aponeurosis which extends from the Vastus medialis, across the femoral vessels to the Adductores longus and magnus; lying on the aponeurosis is the Sartorius muscle. The canal contains the femoral artery and vein, the saphenous nerve, and the nerve to the Vastus medialis.

Even SFA kinematics plays an essential role for stent fractures.

2.4 SFA kinematic studies

At the best of our knowledge, not many scientific studies address the goal to investigate and elucidate the SFA kinematic.
Smouse and his coworkers, in 2005, investigated mainly qualitatively the shortening and bending of bare and stented SFA and popliteal artery using ex-vivo model [31]; in 2006, a more quantitative approach was proposed by Cheng and his group studying the SFA deformation by MR Angiography [33].

In the following two sections we will briefly review these two studies, highlighting and discussing the aspects related with our investigation.
Then, another more recent study [34] by Nikarov et al. was review. As Cheng and his coworkers' study, it wants to characterize the types and the ranges of stent distortion theoretically produced by extremity movement but also to use these ranges as parameters for in vitro long-term fatigue testing of commercially available self-expanding nitinol stents.

2.4.1 Biomechanical forces in the Femoropopliteal Arterial Segment

In this article, Smouse and his coworkers [31] evaluated the morphologic changes occurring in the SFA and popliteal arteries during passive limb movements (walking, stair climbing, sitting-to-standing movement) using a cadaver model. They used 14 limbs of cadavers imaged in the supine, neutral or in the straight-leg position. Then, the hip was flexed

and the knee bent to simulate the several motion type. In Tab. 2.1 we can see the results obtained.

Motion type	Knee bending [degree]	Hip flexion [degree]
straight-leg position	0	0
Walking	70	20
Stairs climbing	90	90
Sitting-to-standing	90	90

Tab. 2.1: Motion and angle flexion of hip and knee of cadaver model.

Flexion and bending angle are defined following the indications provided by Goswami et al [36]. To assist the length measure changes, arterial branches points and short balloon expandable stents were used (Fig. 2.5).

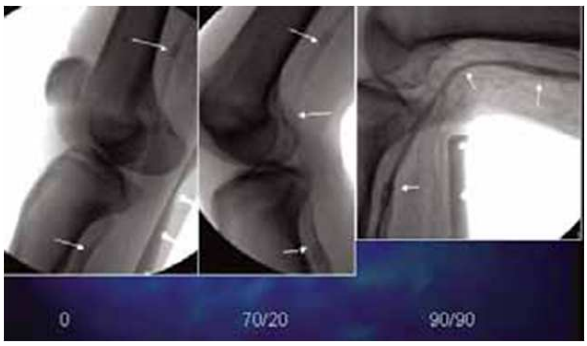

Fig. 2.5: Proximal and distal arrows point to short balloon-expandable stents placed into the popliteal artery to assist with length measurements.The middle arrow shows bending of the popliteal artery with joint movement.

During the above mentioned movements, from the mid SFA to the distal popliteal artery, the authors recorded the following measurements:

- shortening or elongation [mm] ;
- curvature changes [mm of radius];

- degrees of bending of the arterial segments and joints;

Torsion was not critically evaluated because not evident during the study.
All measurements and motions were firstly performed with bare vessels and then repeated after nitinol stent implantation in the SFA and popliteal arteries.
Two different commercially available nitinol stents were applied:

- a more flexible, axially less rigid stent;
- a less flexible stent, 4 times more rigid than the first one.

Both stents had similar surface finishes and radial strengths.

Bare arteries: results and discussion

The authors analyzing the results (Tab. 2.2) about the hip and knee flexion concludes that the SFA and popliteal arteries experience axial compression and bending, with most of the bending occurring behind the knee.

Bare arteries				
Motion type	Mid SFA	Distal SFA	Popliteal	Popliteal bending radius /angle
Walking (70°/20°)	5%	14%	9%	-
Stairs climbing (90°/90°)	10%	23%	14%	13mm/63°

Tab. 2.2: Bare arteries during hip flexion and knee bending.

The magnitude of these changes are related to the magnitude of flexion and bending. There was no elongation, or twisting and no significant bending was observed in the straight segment of the SFA. Although the majority of bending is behind the knee, also in the straight segment of the SFA bending phenomenon will take place when the segment has axially compressed as much as possible, so it will tend to bend or to undulate allowing further foreshortening of the entire segment during ambulation.

Stented popliteal artery with the more flexible stent

In Tab. 2.3 we can observe that there is a reduction of the artery shortening caused by the insertion of the stent.
Following the main idea that the axial rigidity of the artery may influence the bending behavior of the artery, and consequently its capability to accomplish the shortening due to the hip flexion and knee bend, the authors states the following items:

- placing a stenting into the artery adds the undesirable effect of altering the axial rigidity of the vessel;
- depending on the stent type, the vessel rigidity may be drastically increased with the severely reducing of the arteries ability to accommodate foreshortening;
- missing accommodation of foreshortening of the vessels causes an increase of stress in the artery possibly leading to stent kinking or fracturing.

Stented arteries (more flexible stent)			
Motion type	56mm	100m	Bending radius /angle
Walking (70°/20°)	4%	11%	-
Stairs climbing (90°/90°)	7%	14%	20mm/69°

Tab. 2.3: Stented popliteal artery with more flexible stent.

Moreover, keeping the hypothesis that the musculo-skeletal forces applied to the surrounding tissue during joint movement are so great that in an artery with stents will forced to shorten as much as an artery without stents, the authors states the following items:

- there is an inversion relationship between the axial compression and bending above the knee (less axial compression, more bending);
- the bare artery tends to bend in a exaggerated manner adjacent to a rigid stent, maybe speeding up neointimal hyperplasia and/or stent (Fig. 2.6a);

- overlapping stent portions when two or more stents are implanted, the mechanical forces affect overlapping stents differently than single stents with a more compression effect at the margin of overlapped stents and an addition of stress to the stents (Fig. 2.6b);
- during knee bending, stented popliteal artery, since it is not able to accommodate the bending, gets a 3-shape configuration (Fig. 2.6c), leading to a possible stress concentration, instead of bare popliteal artery that bends smoothly (C-shaped configuration);
- with maximum knee bending, the stent can kink as a straw (Fig. 2.6d);

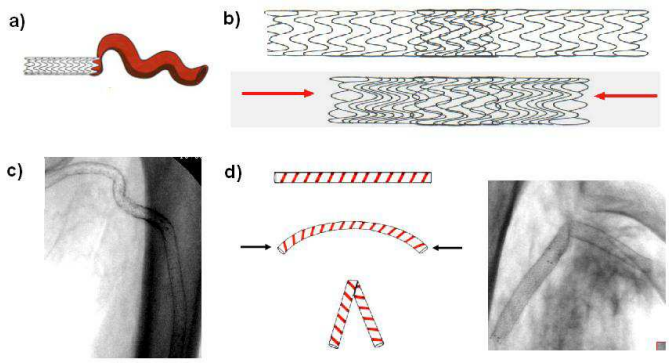

Fig. 2.6: Illustration showing: a) bending of the bare vessel close to stented artery; b) overlapping portion of stents; c) 3-shaped configuration of the stented Popliteal artery; d) Kinking effect of stented popliteal artery at maximum bending.

- there are two stressors affecting stiffness:
  1. bending of the stent behind the knee
  2. uniform radial compression within the straight segment of the SFA and popliteal artery

  Torsion and elongation are not considered significant stressors within implanted stents;
- if two stents, placed next to each other, but not overlapped, and a bare artery gap is left between stents, the stented segments shift into a different plane and ride

over one another, severely deforming the course of the artery (out of plane stent overlap).

2.4.2 In vivo MR quantification of flexion-induced SFA deformation

Cheng and his coworkers [33], in this study, want to quantify in vivo deformation of the SFA in 8 healthy subjects (16 limbs), from the supine position (neutral) to fetal position (maximum hip flexion and knee bend), with the magnetic resonance (MR) angiography use.
With a custom software, from the MR angiographic volume data, the authors reconstructed centerline spline paths for:

- iliofemoral artery;
- profunda femoris;
- descending genicular artery.

Centerline splines are defined as analytical representations of the vessel path that allow a mathematical quantification of the path dimensions.
Soft tissue scans were used to confirm the paths of the iliofemoral artery and its branches. Both arc length of the centerline splines and straight distance between the two point branches of the SFA were computed in supine and fetal positions.
The following measurements were defined:

- SFA stretch: $(arc\ length_{supine}$ - $arc\ length_{fetal})/arc\ length_{supine}$;
- straightness: *100%* - (*arc length* - *straight length*)/*straight length*.

As we can see in Tab. 2.4, SFA was almost completely straight in the supine and fetal positions.

Quantification of the SFA twisting instead requires the determination of:

- the angle of separation between the profunda femoris and descending genicular branches on the SFA for both body position;

- the difference between the two angle of separation.

Method to calculate axial stretch and angle of twist is presented in Fig. 2.7.

Straightness of the SFA			
Position	Arc length [cm]	Straight length [cm]	Straightness [%]
Supine	22.2±3.1	22.0±3.1	99.1±0.4
Fetal	19.2±2.5	19.0±2.5	98.7±0.6
Note: values are presented as means of ± SD.			

Tab. 2.4: Straightness of the SFA for both supine and fetal position.

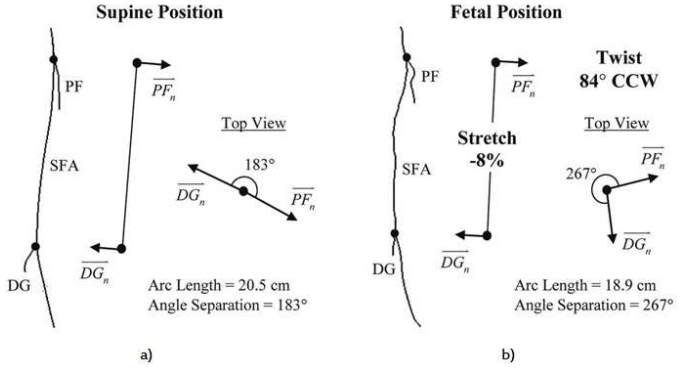

Fig. 2.7: Calculation of SFA axial stretch and angle of twist in a representative left leg. a)Arc length of the SFA and angle of separation between the profunda femoris (PF) normal branch vector ($\vec{PF}_n$) and the descending genicular (DG) normal branch vector ($\vec{DG}_n$) with individual in the supine position. b)Corresponding SFA arc length and angle of branch separation between the PF and DG with individual in the fetal position. The SFA is shortened by 8%, and taking the PF as the reference branch, it twists 84° in the counterclockwise (CCW) direction.

Results

The statistical analysis reveals no significant correlation between SFA arch length and height for either leg or body position. Anyway it should be noted that the selected volunteers have all the same height (164±7 cm).

In Fig. 2.8a we can see that the SFA fetal position arc length (19.2±2.5 cm) was significantly shorter than the SFA supine position length (22.2±3.1 cm) for an average shortening of 13%±11%.

The nearly identical straight length and arc length of the SFA, also evidenced by the near 100% straightness metric of the SFA, demonstrates that we have already said before, i.e. the SFA was almost completely straight in the supine and fetal positions.

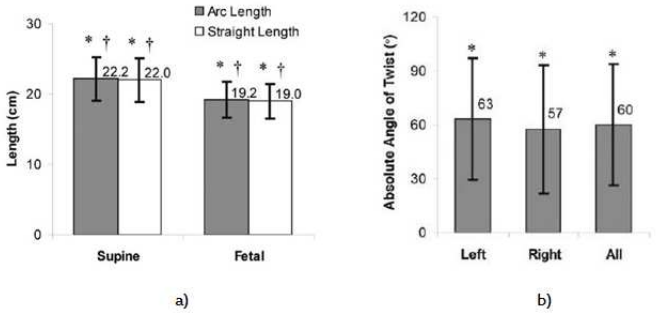

Fig. 2.8: a) Chart of average arc and straight lengths of the SFA with individuals in the supine and fetal positions. Bars denote SDs; asterisk denotes significant difference (P<.05) between arc and straight lengths; dagger denotes significant difference (P<.05) between supine and fetal positions. b) Chart of average absolute angle of twist for the SFA with individuals changing from the supine position to the fetal position. Bars denote SDs; asterisk denotes significant angle of twist (P<.05).

In addition, Fig. 2.8b shows that the absolute angle of twist of the SFA from the supine position to the fetal position was significant for all limbs combined ($60° \pm 34°$) as well as for the left ($63° \pm 34°$) and right ($57° \pm 36°$) sides individually.

2.4.3 Fracture of self-expanding nitinol stents stressed in vitro under simulated intravascular conditions

Nikanorov and his coworkers [34], as Cheng has already done, want to characterize the biomechanical deformations of the femoropopliteal artery but, while Cheng focuses on the bare artery, Nikanorov characterizes the deformation of the stented one in order to obtain parameters for in vitro long-term fatigue testing of commercially available self-expanding nitinol stents.

Firstly, he evaluates native (unstented) arterial deformation in cadaveric lower extremity arteries when the subjects were placed in a supine position and guide catheters were introduced through antegrade access to the common femoral artery. Short sections of balloon expandable stents were placed in the arterial lumen proximal and distal to the area of measurement to serve as radiopaque reference points. Measurements were taken at:

- a neutral position (straight leg assuming 0° or no flexion in knee and hip joints);
- a bending angle of 110° (knee flexion of 70°) and at a bending angle of 160° (hip flexion of 20°);
- at 90° knee and hip flexion angle.

70°/20° position represents *walking* while 90°/90° position represents *sitting-to-standing* or *stair climbing*, founded to be good approximations. [36]
Results summarized in Tab. 2.5 show that the distal-SFA/prox-PA region appeared to be the most critical area for shortening, with the highest percent axial compression, at 23%±2% with 90°/90° knee/hip flexion, that is more than twice the 9%±5% observed in the mid-SFA under the same conditions.

Position	Mid SFA	Distal-SFA/Prox-PA	PA
Neutral (%)	0	0	0
Knee/hip flexion			
70°/20° (%)	5±4	14±5	9±5
90°/90° (%)	9±5	23±2	14±3

Tab. 2.5: Axial compression of cadaveric lower extremity unstented arteries induced by knee and hip flexion.

Then, he assesses the self-expanding stent deformation.
Six different stents' type of 100 mm length were deployed in SFA or popliteal artery (PA), or in both arteries of the cadavers and post-dilated with a balloon catheter to ensure good

apposition to the arterial wall and to simulate the clinical setting.
For the purpose of measurement, the artery was separated into three segments:

- middle SFA (mid-SFA);
- distal-SFA/prox-PA;
- PA.

For each implanted stent, in particular, the following lengths were determined:

- at neutral (0°) position;
- at flexion of 70°/20°;
- at flexion of 90°/90°.

The primary measurements from lateral view images were of stent shortening (edge-to-edge) and deflection angle, defined as the bend angle between neutral (defined as 0°) and flexion.
The axial compression of this self-expanding nitinol stents is summarized in Tab. 2.6.

Finally, due to results obtained, fracture after repetitive in vitro axial compression and bending deformation are evaluated for all six stents, using a specially designed bend fatigue test machine wherein stents were housed in elastic silicone tubing with a wall thickness of 3.0±0.2 mm.

Position	Mid SFA	Distal-SFA/Prox-PA	PA
Neutral (%)	0	0	0
Knee/hip flexion			
70°/20° (%)	3±2	4±1	6±4
90°/90° (%)	3±3	6±3	11±5

Tab. 2.6: Axial compression of 100-mm self-expanding nitinol stents when placed in cadaveric lower extremity arteries.

Conclusion

The first study analyzed [31] has several limitation factors: use of ex-vivo model, limited sample size, non-atherosclerotic limbs, passive movement, no crossing of legs or limb twisting, no hyperextension or elongation, and tested with only two stent types. Despite this, however, the investigation is useful to conclude that:

- the ideal stent design would be made up of a series of independent flexible rings (not interconnected) in order to provide radial support even if without impeding or altering the physiologic axial compression and bending normally found in an artery with ambulation and positional changes.

From the results obtained in the second study [33] the authors postulated that:

- stents with greater axial and torsional flexibility would have better fatigue characteristics.

As for the third study [34], it's so possible to conclude that:

- self-expanding nitinol stents undergo both axial and bending deformation when implanted into the superficial femoral and popliteal arteries
- commercially available stents exhibit a variable ability to withstand chronic deformation in vitro, and that their response is highly dependent on the type of deformation applied

As we can see, self-expanding Nitinol stent seems to be a good choice in treating SFA disease.
However, fatigue fracture occurrences of up to 50% have been reported in some stents after one year [44].
So in the following chapter we will describe Nitinol and its main features but also what is fatigue and how the fracture process takes place.

Chapter 3

Nitinol and Fatigue

In the previous chapter, we have discover that Nitinol self-expanding stents have become effective in treating SFA disease.
In the following sections therefore it seems reasonable to describe Nitinol properties, the fatigue and the fracture process.

3.1 Nitinol main features

Nitinol is a **shape-memory alloy** of roughly 50% Nickel and 50% Titanium.

Discovered only in 1960s as part of a Naval research project [45], Nitinol derives its name from its chemical components and its founders: Ni (Nickel) + Ti (Titanium) + NOL (Naval Ordinance Lab).

It has good **biocompatibility** (response is similar to stainless steel) and **good magnetic resonance imaging opacity** (i.e. can readily be seen by X-ray or MRI), making it ideally suited for design of biomedical implantable devices [46]-[50].

The most important characteristics that make Nitinol extraordinarily unique from other bioengineering metallic alloys are:

- **shape-memory effect**;
- **superelasticity**;
- **fatigue resistance**.

3.1.1 The Shape Memory Effect

A shape memory alloy (SMA) belongs to a class of solids that can undergo reversible solid-solid phase transitions between a crystallographically more-ordered phase, called *austenite* and a crystallographically less-ordered phase, called *martensite*. This function of SMA was defined as the shape memory effect (SME).
Generally, it is believed that the SME results from the thermoelastic martensitic transformation.
The schematic micro mechanism of the SME is shown in Fig. 3.1 where we define M_s, M_f, A_s and A_f as the starting and finishing temperature of martensitic and austenitic transformation.
The martensite will be produced when the parent austenite crystal is cooled below the M_s. At this stage, there will be no macro shape change because of the coordinately twinned deformation, called self-accommodation. Twinned boundaries will move and disappear when the martensite undergoes extra stress at a temperature below M_f, which results in macro deformation (Fig. 3.1b). On heating to the A_s temperature, the deformed martensite will resume the original shape of the parent through the reverse transformation from the martensite to the parent austensite phase [51, 52].

To better understand how nitinol behaves at macroscopic level we can refer to Fig. 3.2 where a nitinol tube is firstly deformed at low temperature and then heated to make it back in its original shape.

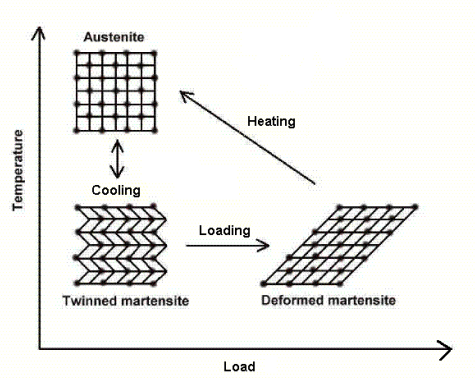

(a)

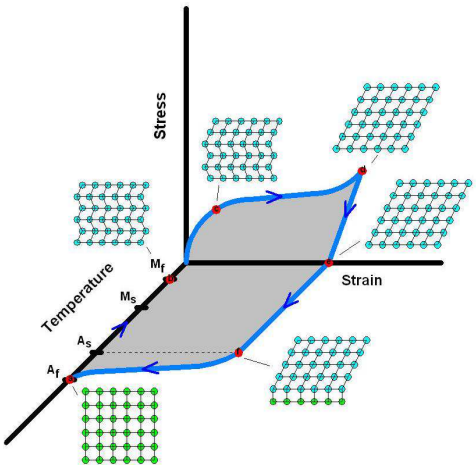

(b)

Fig. 3.1: SME micro mechanism. A)Transformation from the austenite to the martensite phase and shape memory effect. The high-temperature austenitic structure undergoes twinning as the temperature is lowered. This twinned structure is called martensite. The martensitic structure is easily deformed by outer stress into a particular shape, and the crystal structure undergoes parallel registry. When heated, the deformed martensite resumes its austenitic form, and the macroscopic shape memory phenomenon is seen.

B) At high temperature (a), the material is fully austenite. Lowering the temperature below the Mf (b) without the addition of stress causes a phase transformation to twinned martensite. As the martensite is loaded, it begins to detwin (c), until full detwinning has occurred (d). Upon unloading to (e), the martensite elastically recovers, but does not return to a twinned state. Raising the temperature to the austenite start temperature, As (f), begins the reverse transformation from martensite to austenite, which is complete at Af (a).

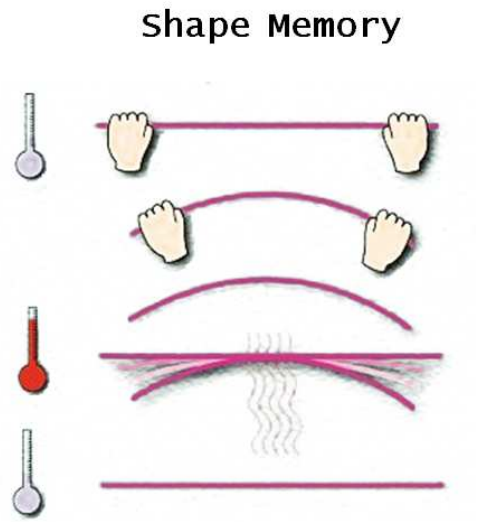

Fig. 3.2: SME macro mechanism. A nitinol tube in its initial configuration was firstly deformed at low temperature and then heated to go back it to its original shape [53].

3.1.2 Superelasticity and Hysteresis

The superelasticity of nitinol was the predominant property to use in stent applications. Superelasticity (or pseudoelasticity) refers to the ability of NiTi to completely recover, upon unloading, its original shape (elastic) and to the fact that the transformation strains are so large (of the order of 6%) compared to the typical elastic strains in a metal (of the order of 1%) (superelastic). This is based on stress-induced martensite formation. At rest, the material present itself in an austenite phase, which behaves linearly elastically.
Upon loading at a temperatures higher than M_s, this austenite phase transforms into a martensite phase which is also linear elastic but with a different elasticity constant. The transformation produces a substantial amount of strain and is triggered by stress, over a relatively narrow range.
Upon unloading, the transformation is reversible. However, the stress levels at which such reversible transformation occurs are smaller than the stresses required to produce the original transformation (Fig. 3.3). If a reverse loading is applied (for instance in compression instead of tension), a similar behavior is observed, with the exception that, to produce the transformations, the stress levels required are higher, while the strain are lower (hysteresis behavior).

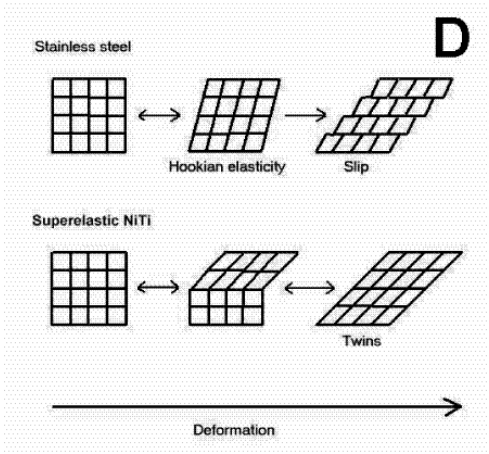

(a)

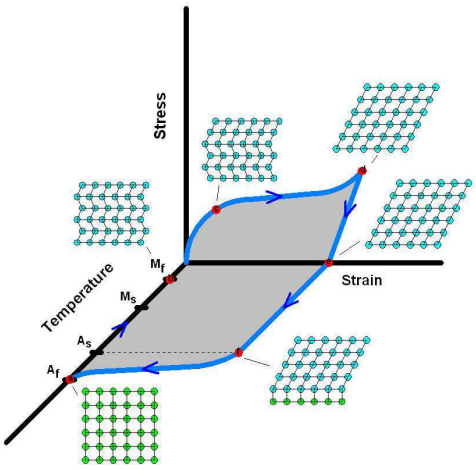

(b)

Fig. 3.3: Schematic of superelastic effect. At temperatures above the austenite finish temperature, A_f, but below the martensite deformation temperature, M_d, the superelastic effect occurs in Nitinol. Starting at (a) the material is fully austenite. The austenite is elastically loaded to point (b) at which time transformation to martensite occurs (the martensite forms in twins, and instantaneously detwins due to the high applied stresses). Further loading along a stress plateau to point (c) fully transforms the material to martensite. Continued loading to (d) requires increased stress and elastically deforms the martensite (note that the SIM elastic modulus is lower than the austenite modulus of elasticity). Unloading back through point (c) recovers the elastic strains in the martensite, and continued unloading to (e) forces the onset of the reverse transformation to austenite, with full reverse transformation upon complete unloading to (a).

This hysteresis is a desirable feature in stent design as a superelastic stent should provide a very low *chronic outward force* (COF) against a vessel wall, and at the same time an highly resistance to crushing-compliant in one direction, and stiff in the other.

Even for this property, in Fig. 3.4 we can see the macro mechanism of superelasticity effect. The tube is deformed and, if released, it returns to its initial configuration.

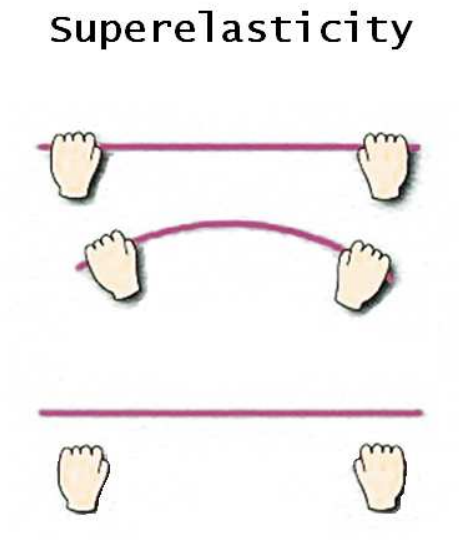

Fig. 3.4: SE macro mechanism. The tube if deformed and then released returns to its original shape [53].

3.1.3 Fatigue resistance

The fatigue behavior of Nitinol has recently gained a lot of attention driven by its application in bad environments, such as in superficial femoral arteries and in percutaneous heart valve replacement and repair [44, 54]-[56].
Much work has been done to characterize the fatigue performance of nitinol, both in *strain-* and *stress-controlled* environments. Material fatigue, in fact, is typically evaluated based on stresses or strains.
Strain based approach is used to describe environments in which a device is alternately deformed between two set shapes, while stress approach to describe the influences of cyclic loading.

In the body most fatigue environments involve irregular cyclic motion against highly compliant tissue, becoming so a combination of stress- and strain-control.
Moreover fatigue is usually complicated even by the superposition of a mean stress or strain on the top of the cyclic component [50], but it's important to note that, contrary to that observed in conventional engineering materials, Nitinol fatigue life is not limited by the magnitude of the mean strain. It is even observed that fatigue life increases with the increase of the mean strain and that the oscillating strain amplitude becomes the main contributor to fatigue behavior [57, 58]
In our study so we cannot consider the mean strain effect and we'll treat only the zero-mean strain condition; this is not clinically relevant but provides a basis for comparison with great mean strains.

In the following section, anyway, we'll learn more about the fatigue concept introducing also the approach to study it.

3.2 Fatigue and crack propagation

Fatigue can be defined as a gradual damaging of the structural detail under cyclic loads. Gradual damaging occurs in the form of local material failures leading to fatigue crack propagation. The first two stages of fatigue crack propagation, *crack initiation* and *stable crack growth*, substantially contribute to the fatigue life of the detail while the third stage, *unstable crack growth*, can be ignored since it is short compared to the other two.

The cause of a local material failure is a cyclic stress field leading to cyclic strain in the material. If the cyclic strain is high enough, the micro-cracks nucleate at micro-structural defects, grow and join together leading to local material failure. The process of *nucleation*, *growth* and *joining* of micro-cracks takes place in zones where high stress concentrations prevail. These zones are usually situated around geometrical discontinuities named stress concentrators (so called due to their ability to concentrate stress around them) that can be divided into two groups:

- crack initiators (holes, welds and notches);
- fatigue cracks.

It can be shown that crack initiation occurs due to local material failure at the crack initiators, and that stable crack growth is due to material failure at fatigue crack tip.

Critical conditions for the growth of a crack (Fig. 3.5) can be formulated in more precise terms by means of ***Linear Elastic Fracture Mechanics*** [59].

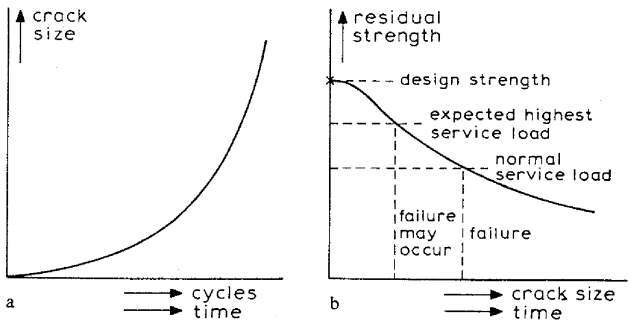

Fig. 3.5: a) Crack propagation as a function of time; b) shows that the residual strength of a structure decreases progressively with increasing crack size.

3.2.1 Linear Elastic Fracture Mechanics (LEFM)

The theory of cracking phenomena or *fracture mechanics* describes the behavior of solids or structures with macroscopic geometric discontinuities at the scale of the structure. These discontinuities are lines in two-dimensional media (such as plates and shells) and surfaces in three-dimensional media.
In the structural analysis these discontinuities must be taken into consideration as they modify the stress, strain and displacement fields.

As early as 1920, Griffith showed that the failure of a brittle elastic medium could be characterized by a variable, later called the *energy release rate*, whose critical value, independent of the geometry of the structure, was a characteristic of the material. This approach, called *the global approach*, showed that in all cases the essential phenomena occurs closeness to the crack front and that it is possible to study the macroscopically cracked medium with the help of intrinsic variables. This is due to the high stress concentration present at the tip of a crack which, for linear elasticity, can be represented by singularity of the stress field.

The base of LEFM is an elastic analysis of the stress field for small strains and gives excellent results for brittle-elastic materials like high-strength steel and glass.
With the occurrence of plasticity or viscoplasticity we enter into the field of *non linear fracture mechanics*. This is the case for ductile materials like stainless steel, some alluminium alloys and polymers. The plasticity manifests itself in two ways:

- at the level of the plastic zone in front of the crack tip as it is the source of an history effect by virtue of the development of residual stresses and
- at the level of the mechanism of crack propagation by superposition of the mechanism of ductile fracture, that arises from the instability resulting when large local deformations occur in the vicinity of crystalline defects.

As long as the load is low enough, whether monotonically increasing or periodic, these effects can be neglected and LEFM continues to provide a good approximation to the physical reality.
In contrast, for large and highly variable loads, the stable progression of ductile fracture cracks and the history effects due to overloads can be modeled only by taking plasticity into account.
Anyway, although a plastic or damaged zone is always present at the crack tip, it will be seen that linear elastic analysis provides a sufficiently accurate representation of the reality.

The first assumption of fracture mechanics is that, in the structure under consideration, an initial crack and a system of external loads exist. The initial crack can be either a crack created by damage under the effect of these loads, or a defect created during the manufacture or forming of the material. In the first case, it will be progress by continuation of the damage mechanism [60] while, in the second case, there is no relation between the crack orientation and the loading system.

There are three ways to open a crack (Fig. 3.6):

- **Mode I** that is the *tensile opening mode*;
- **Mode II** that is the *in-plane sliding mode*;
- **Mode III** that is the *tearing* or *anti-plane shear mode*.

Mode I, however, is the most important because:

- at equal crack length, it triggers fracture for values less than the nominal stress
- the fracture plane, in the crack growth phase, is perpendicular to the applied stress.

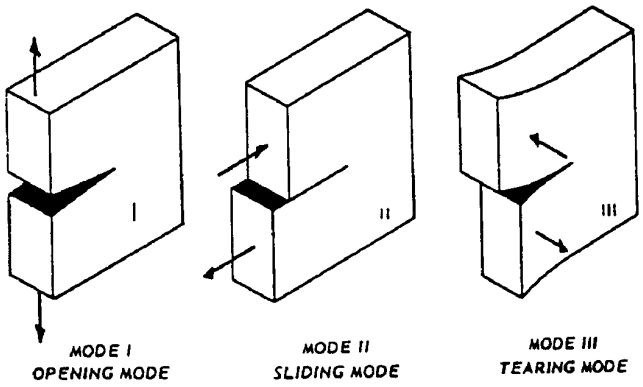

Fig. 3.6: In **Mode I** the crack faces separate in a direction normal to the plane of the crack and the corresponding displacements of the crack walls are symmetric with respect to the x-z and the x-y planes. In **Mode II** the crack faces are mutually sheared in a direction normal to the crack front. Here the displacements of the crack walls are symmetric with respect to the x-y and anti-symmetric with respect to the x-z plane.
In the **Mode III** the crack faces are sheared parallel to the crack front and the displacements of the crack walls are anti-symmetric with respect to the x-y and the x-z planes.

Once a crack is present, its initiation advances under monotonic, quasi-static loading conditions. A way of characterizing the singularity of the stress field in the vicinity of the crack tip is to characterize it by the critical value of a scalar parameter, the *stress intensity factor* (K) [59].

The stress intensity factor

Stress intensity factor is a parameter independent of the crack location that varies only with the load and the crack half-length. It is defined as:

$$K = \beta\sigma\sqrt{\pi a} \tag{3.1}$$

where:

- β is a geometric factor that depends on the geometry of the structure (for a infinite plate, mode I, $\beta = 1$);
- σ is the stress applied to the structure;
- a is the semi crack length.

Its critical value, K_c, is a function of the mode loading, chemical environment, material microstructure, test temperature, strain rate, and state of stress (i.e. plane stress or plane strain) and it's determined through experimental tests on specimens that must conform to the requirements of small-scale yielding [1] and other conditions which are spelled out in detail in the fracture standard E-399 developed by the American Society for Testing and Materials (Philadelphia) in 1974 [59].

Another global approach consists instead in studying the balance of the energies taking part in the crack growth process. The parameter defined from this balance is named *strain energy release rate* (G).

The strain energy release rate

For purely brittle fracture originating from a crack whose length is a and existing in a body subjected to an applied stress σ, Griffith postulated that the critical rate of strain energy released during unstable crack extension, G_c, is related to the surface energy of the material, γ, as:

$$G_c = 2\gamma = \frac{\pi \sigma_c^2 a}{E} \tag{3.2}$$

where:

- σ_c is the critical stress at the onset of fracture;
- E is the elastic modulus

[1] **Small scale yielding:** condition requiring that plastic zone size is much smaller than the crack size

$$\left(\frac{K_c}{\sigma_y}\right)^2 << a$$

Irwin showed moreover that G can be related with K through this equation:

$$G = \frac{K^2}{E} \tag{3.3}$$

even if the relationships are strictly applicable to brittle materials in which the energy dissipation due to the plastic deformation is almost negligible. Many structural materials show, instead, evidence of plastic deformation and have fracture toughness (K_{Ic}) levels higher than those that can be estimated from surface energy alone.
Hence the modified form of Eq. 3.2 to account for this additional contribution to fracture resistance due to plastic deformation can be written as:

$$G_c = \underbrace{2\gamma}_{elastic} + \underbrace{\Gamma\sigma_y\delta_c}_{plastic} \tag{3.4}$$

where:

- Γ is a constant;
- σ_y is the material yield stress;
- δ_c is the critical opening displacement at the crack tip at the onset of fracture.

The first term is the energy dissipated in the creation of two fracture surfaces during fracture and is considered independent of microstructure while the second term, $\sigma_y\delta_c$, represents approximately the energy dissipated in plastic deformation causing fracture, a strong function of microstructure. Because the latter is severals times higher than the former, the surface energy term is often neglected in the case of metallic structural materials [61].

For our application, we can assume to have a brittle fracture as in a Nitinol stent, once a crack is nucleated catastrophic failure rapidly ensues because of the small cross sections. Moreover, as we will describe in Chapter 4, the program we will use to simulate and study the crack propagation provides a criterion based on this parameter.

Part II

Numerical Simulations

Chapter 4

Crack and crack propagation study with ABAQUS

After the previous introductive chapters we want now start to discuss our application. Here, in particular, the commercial software used, ABAQUS, and how study the crack propagation problem with it are presented. The chapter ends with some examples helping us to better understand the more complex problem we'll treat in the Chapter 5.

4.1 Introduction

ABAQUS [63] is a finite element (Appendix A) system that includes severals programs:

- **Abaqus/Standard**, an implicit finite element program;
- **Abaqus/Explicit**, an explicit dynamics finite element program;
- **Abaqus/CAE** (Fig. 4.1), an interactive environment used to create finite element models, submit Abaqus analyses, monitor and diagnose jobs, and evaluate results; and
- **Abaqus/Viewer**, a subset of Abaqus/CAE that contains only the postprocessing capabilities of the Visualization module.

Abaqus/Standard and Abaqus/Explicit can be run as batch applications or through the interactive Abaqus/CAE environment. The main input to the Abaqus/Standard and Abaqus/Explicit analysis products is a file containing the options required for the simulation and the data associated with those options. The input file is usually created by Abaqus/CAE or another preprocessor (pyFormex [64], for example).

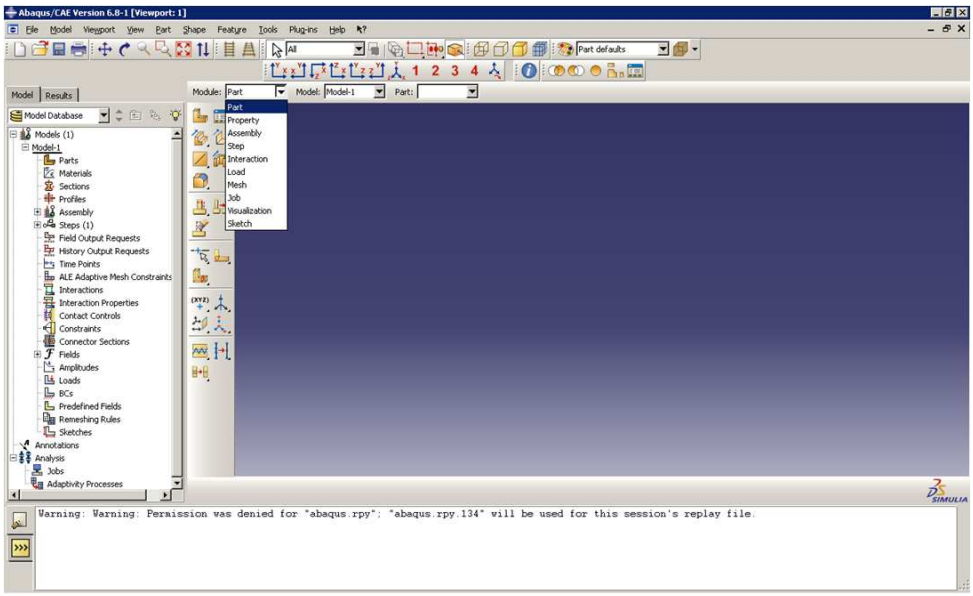

Fig. 4.1: Abaqus/CAE: a simple, consistent interface for creating, submitting, monitoring, and evaluating results from Abaqus/Standard and Abaqus/Explicit simulations. Each module defines a logical aspect of the modeling process (ex.defining the geometry, defining material properties, and generating a mesh); moving from module to module, the model is built and from this one, Abaqus/CAE generates an input file that is submitted to the Abaqus/Standard or Abaqus/Explicit analysis product. The analysis product performs the analysis, sends information to Abaqus/CAE to allow monitor the progress of the job, and generates an output database. Finally, using the Visualization module it's possible to read the output database and view the results of the analysis [65].

For our study, we'll use Abaqus/Standard program as it allows to analyze both the **onset of cracking** and the **crack propagation** problem. In particular:

- the onset of cracking can be studied in quasi-static problems by using contour integrals ("Contour integral analysis", Section 4.2), in two- or three-dimensional problems but the crack propagation cannot be studied because focused meshes are generally required;

- the crack propagation allows a quasi-static analysis of the crack growth along predefined paths ("Crack propagation analysis", Section 4.3).

In the following sections we'll review the methods available for both of the two problems with reference to the ABAQUS Documentation [65]. However, as our aim is to study the crack propagation in a stent, in the next chapter we'll focus especially on the second one.

4.2 Contour integral evaluation

Contour integrals are output quantities, valid in two and three dimensions, that can be requested only in general analysis steps. Several contour integral evaluations are possible at each location along a crack. In a finite element model each evaluation can be thought as the virtual motion of a block of material surrounding the crack tip (in two dimensions) or surrounding each node along the crack line (in three dimensions). Each block is defined by *contours* each of which is a ring of elements completely surrounding the crack tip, or the nodes along the crack line, from one crack face to the opposite crack one. These rings of elements are defined recursively to surround all previous contours.

Abaqus/Standard offers the evaluation of several parameters for fracture mechanics studies:

- the J-integral, widely accepted as a quasi-static fracture mechanics parameter for linear material response and, with limitations, for non-linear material response;
- the C_t-integral, which has an equivalent role to the J-integral in the context of time-dependent creep behavior in a quasi-static step;
- the stress intensity factors ($K_{I,II,III}$), used in linear elastic fracture mechanics to measure the strength of the local crack-tip fields (Section 3.2.1);
- the crack propagation direction, i.e. the angle at which a pre-existing crack will propagate;
- the T-stress, represented a stress parallel to the crack faces and is used as an indicator of the extent to those parameters that, like the J-integral, are useful characterizations of the deformation field around the crack.

The first step of this method is to define the crack in order to perform then a contour integral analysis. So the crack front, the crack tip or crack line, and the crack extension direction must be selected. In some cases the crack tip or the crack line is the same as the crack front selected, and Abaqus/CAE selects the crack tip or crack line for us.
A crack in a two-dimensional model can be seen as a region containing *edges* free to move apart while in a three-dimensional model is a region containing *faces* free to move apart. The simplest approach to performing a contour integral analysis uses a region that already contains edges or faces that are free to move apart as the crack separates. Alternatively, the crack can be modeled as a line embedded in a face, in a two-dimensional model, or as a face embedded in a cell, in a three-dimensional model. The embedded line or face is called **seam**, and it can be possible to perform a contour integral analysis using it. When the model is meshed, Abaqus/CAE creates duplicate overlapping nodes on the seam; these coincident nodes are free to move apart as the seam separates (Fig. 4.2).

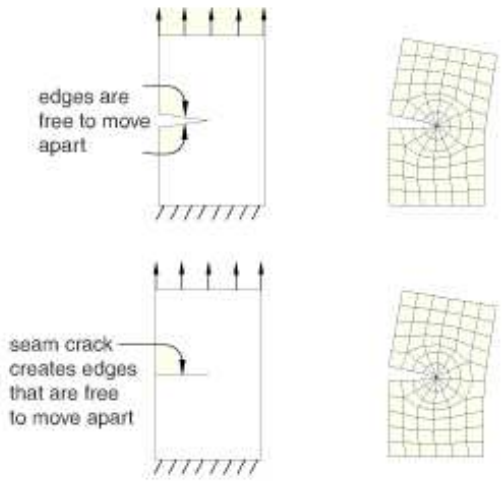

Fig. 4.2: A crack defined using an existing region or using a seam.

In order to further clarify the previous idea, in the following figures (Fig. 4.3 and Fig. 4.4) we can see two examples of contour analysis: the first without the use of the seam and the second with it.

The crack front, the crack line, and the crack extension direction are defined in the Interaction module of Abaqus/CAE while, the number of contours and the type of output

(J-integral,K ...)must be defined in the Step module.

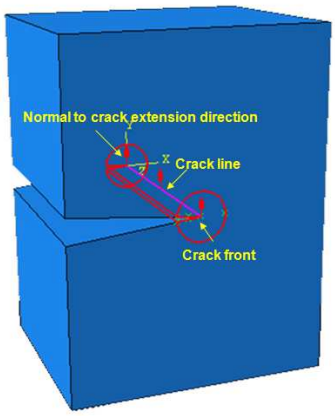

(a)

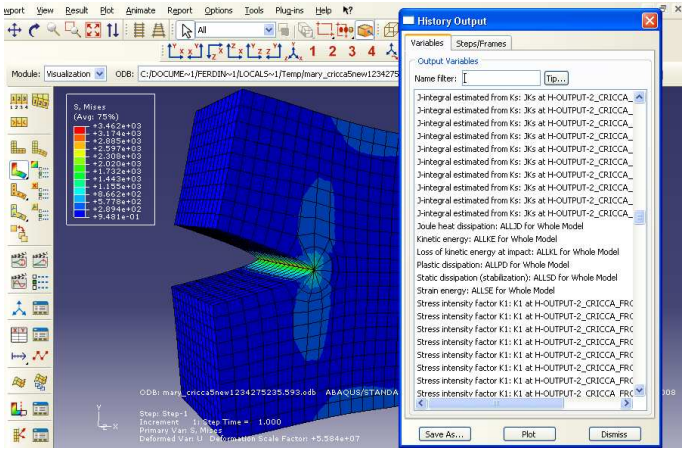

(b)

Fig. 4.3: a) Crack front, crack line, and crack extension direction definition without the seam definition. b) Mesh and contour analysis.

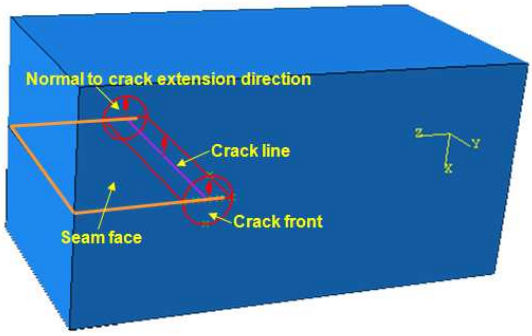

(a)

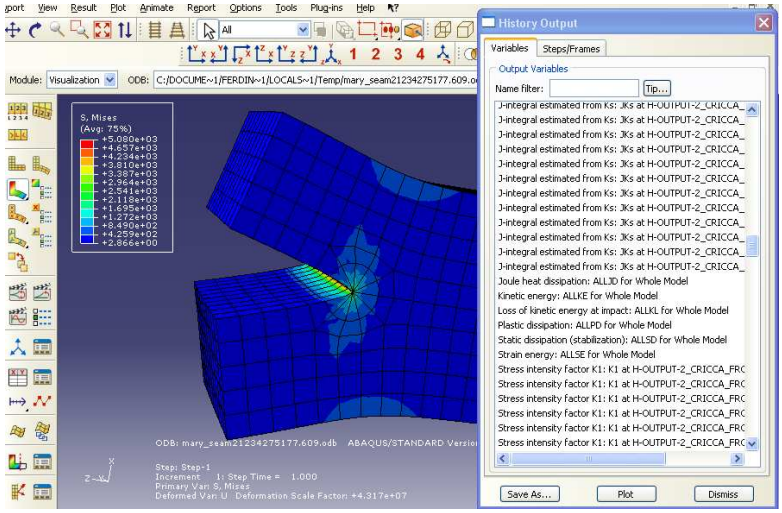

(b)

Fig. 4.4: a) Crack front, crack line, and crack extension direction definition with the seam definition. b) Mesh and contour analysis.

4.3 Crack propagation analysis

This analysis type bases itself on the idea that cracks debond along two user-defined surfaces (slave and master).
The predetermined crack surfaces are assumed to be initially partially bonded so that the crack tips can be identified directly by Abaqus/Standard. To identify which part of the crack is initially bonded it's necessary to define an initial condition specifying:

- a slave surface;
- a master surface;
- a node set that identifies the initially bonded part of the slave surface. The unbonded portion behaves as a regular contact surface.

If the crack propagation capability is activated the two initially partially bonded surfaces separate.
If not, the specified initial contact conditions would have the same effect as that provided by the tied contact capability, generating a permanent bond between the two surfaces during the entire analysis.
To activate the node debonding, this analysis proposes five types of fracture criteria:

- critical stress at a certain distance ahead of the crack tip;
- critical Crack Opening Displacement (COD);
- crack length versus time;
- Virtual Crack Closure Technique (VCCT);
- low-cycle fatigue criterion;

All discussed types are available for crack growth analysis in two dimension, but only the last two criteria can be used in three dimensional problem since our problem is three dimensional we must choose one of the two last criteria. Moreover it is an high-cycle fatigue problem[1] so, the only criterion we can use is the VCCT one.

[1]Fatigue testing on stents requires that 10 million cycles were achieved. This means that the test is conducted in High-Cycle fatigue (number of cycles $\geq 10^5$).

4.3.1 VCCT criterion

The VCCT criterion uses the principles of linear elastic fracture mechanics (LEFM) and, therefore, is appropriate for problems in which brittle crack propagation occurs along predefined surfaces. It is based on the assumption that the strain energy released when a crack is extended by a certain amount is the same as the energy required to close the crack by the same amount.
In the general case, the fracture criterion is defined as:

$$f = \frac{G_{equiv}}{G_{equivC}} \geq 1 \tag{4.1}$$

where:

- G_{equiv} is the equivalent strain energy release rate calculated at a node;
- G_{equivC} is the critical equivalent strain energy release calculated based on the user-specified mode-mix criterion and the bond strength of the interface.

The crack-tip node debonds when the fracture criterion reaches the value of 1.0.
In figure Fig. 4.5, for example, if we consider only the Mode I crack opening, nodes 2 and 5 start to release when

$$f = \frac{G_I}{G_{IC}} = \frac{1}{2}\left(\frac{v_{1,6}F_{v,2,5}}{bd}\right)\frac{1}{G_{IC}} \geq 1$$

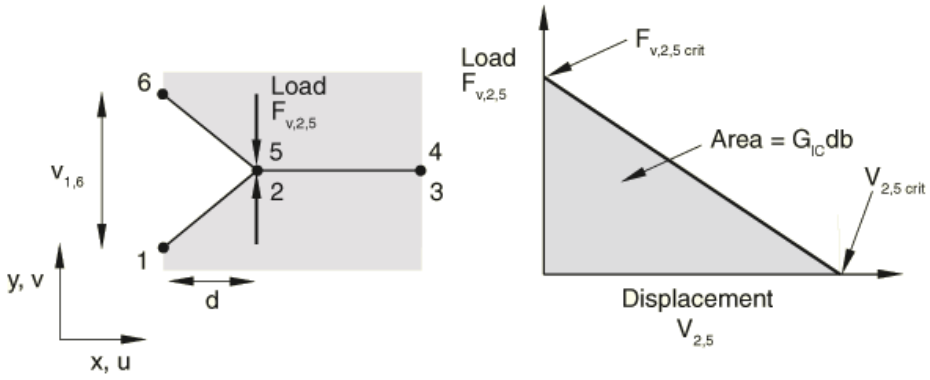

Fig. 4.5: Application of VCCT criterion for Mode I crack opening.

where:

- G_I is the Mode I energy release rate;
- G_{IC} is the critical Mode I energy release rate;
- b and d are the width and the length of the elements at the crack front;
- $F_{v,2,5}$ is the vertical force between nodes 2 and 5;
- $v_{1,6}$ is the vertical displacement between nodes 1 and 6.

For computing G_{equiv}, Abaqus/Standard provides three common mode-mix formulae:

- the BK law model [66];
- the power law model [67];
- the Reeder law model [68].

BK law

The BK law model is described by Benzeggagh (1996) with the following formula:

$$G_{equivC} = G_{IC} + (G_{IIC} - G_{IC}) \left(\frac{G_{II} + G_{III}}{G_I + G_{II} + G_{III}} \right)^{\eta} \tag{4.2}$$

where both G_{Ic}, G_{IIc}, G_{IIIc} and η, semi-empirical criterion exponent, depend on the material type and η, in particular is even independent to the displacement rate of loading; if we have a brittle material, η=2, while if the material is ductile, η=3.
The model anyway provides a power law relationship combining energy release rates in Mode I, Mode II, and Mode III into a single scalar fracture criterion.

Power law

The power law model is described by Wu (1965) with the following formula:

$$\frac{G_{equiv}}{G_{equivC}} = \left(\frac{G_I}{G_{IC}} \right)^{am} + \left(\frac{G_{II}}{G_{IIC}} \right)^{an} + \left(\frac{G_{III}}{G_{IIIC}} \right)^{ao} \tag{4.3}$$

Reeder law

The Reeder law model is described by Reeder (2002) with the following formula:

$$G_{equivC} = G_{IC} + (G_{IIC} - G_{IC}) \left(\frac{G_{II} + G_{III}}{G_I + G_{II} + G_{III}} \right)^{\eta} + \\ + (G_{IIIC} - G_{IIC}) \left(\frac{G_{III}}{G_{II} + G_{III}} \right) \left(\frac{G_{II} + G_{III}}{G_I + G_{II} + G_{III}} \right)^{\eta} \tag{4.4}$$

The Reeder law is best applied when $G_{IIC} \neq G_{IIIC}$. When $G_{IIC} = G_{IIIC}$, the Reeder law reduces to the BK law.
Reeder law can be applied only to three-dimensional problems.

For our application we have chosen to use a BK law because, as we'll see in the following chapter, G_{IIC} and G_{IIIC} may have the same values.

A three dimensional example of crack propagation using VCCT criterion and the BK law to computing the value of G_{equivC} can be seen in Fig. 4.6 and Fig. 4.7.
The steps performed were:

- creation of the 2 solid parts with the definition of the material (steel);
- selection of the master and the slave surfaces and of the node set that identifies the initial bonded part of the slave surface;
- definition of the initial conditions;
- definition of the fracture criterion to use (VCCT combined with the BK law) and of its parameters (G_{Ic}, G_{IIc}, G_{IIIc} and η);
- application of the boundary conditions and the displacement on the nodes of the upper surfaces of the two parts created (Fig. 4.6).

Initially the value of the criterion parameters were chosen with reference to an example of the ABAQUS examples manual [69]. Whit these values, however, the analysis had not convergence as G_{equiv} resulted much more higher than G_{equivC}. So the parameters value has been adjusted in order to have G_{equivC} slightly lower than G_{equiv}. The value of G_{equiv} is calculated as a combination of the values of G_I, G_{II} and G_{III} provided by the program. When we have discovered a good combination of these parameters the analysis has been a convergence and the crack has propagated (Fig. 4.7).

The next chapter shows the application of the criterion on a stent geometry. We will discuss about its geometry definition, the conditions allowed us to applicate the criterion and finally the discussion on the results obtained.

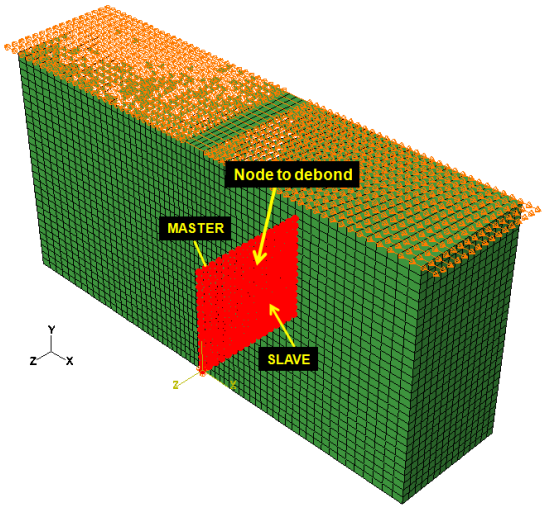

Fig. 4.6: Master, slave and node set definition for the VCCT fracture criterion. On the upper surfaces of the two parts, the orange arrows symbolize the displacements imposed to each node.

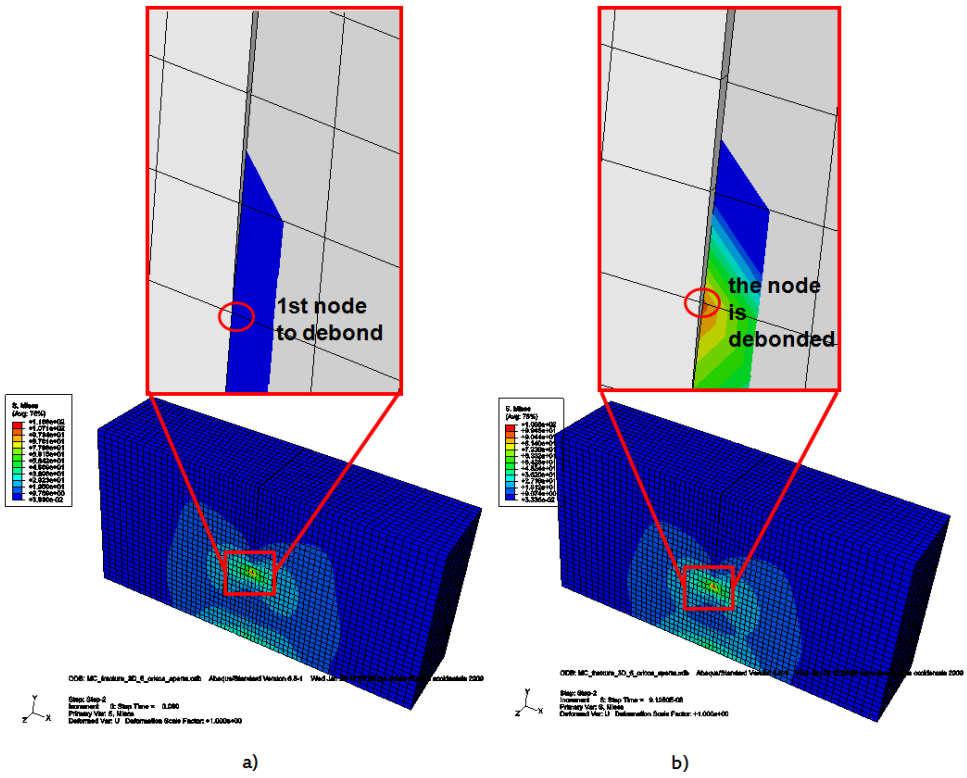

Fig. 4.7: a) Initially the body is intact. A crack is visible and master and slave surfaces are initially tied b) The fracture criterion is satisfied and the crack propagates with the debond of the nodes.

Chapter 5

Crack propagation in a SFA nitinol stent

As we have seen in previous chapters, our study is focusing on the crack evaluation of a Nitinol stent for the SFA disease. Here we'll introduce firstly the S.M.A.R.T.[1] nitinol stent by Cordis, a Johnson & Johnson company in NY, USA [70]. Then we will continue with the description of the stent geometry realization and with the crack propagation study.

5.1 Introduction

SMART stent (Fig. 5.1) is a self-expanding, crush-recoverable nitinol stent for treating blockages in the iliac, or peripheral arteries as well as biliary obstructions within the body. It takes advantage from the superelasticity effect of the material (Section 3.1) so, if extremely deformed (i.e. crimped in a catheter) it recovers its original shape after the removal of the load (i.e. when released into the vessel).

As for the manufacturing process, the SMART stent was made from a Nitinol tube that is:

[1] **SMART:** Shape Memory Alloy Recoverable Technology.

- laser machined;
- cold expanded to its nominal dimension, typically at a diameter many times larger than the original tube diameter;
- annealed[2] to provide its new unloaded configuration that, taking advantage on the superelasticity, was then implanted.

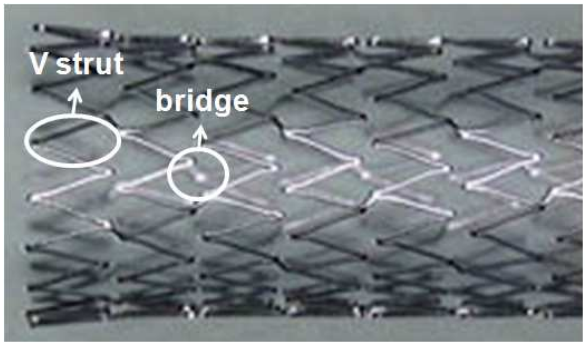

Fig. 5.1: Cordis SMART stent. To note the repeating pattern of "strut Vs" connected by bridges.

To be implanted, in particular, the annealed stent is:

- crimped from the outside and inserted into the delivery system, usually a system of catheter tubes;
- then released to get the contact with the vessel.

In this study, all of these stages are simulated in order to have a good reproduction of the stent behavior.
Giving appropriate boundary conditions, we consider however only one ring as we are interested in founding a possible methodology to characterize the crack propagation and, to do this, there is no need to study the whole stent (Fig. 5.2).

The laser-cutted stent geometry is realized pyFormex a tool for generating, manipulating and transforming large geometrical models of 3D structures by sequences of mathematical transformations.

[2]**Annealing:** heat treatment carried out to remove the surface tensions caused by the manufacturing mechanical process.

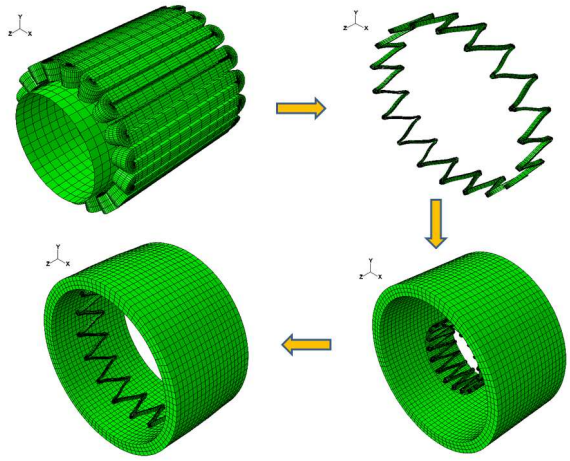

Fig. 5.2: Stent manufacturing simulations for only one ring; *cold expansion* of the laser-cutted stent and *releasing* into the vessel after the *crimping* in a catheter.

The dimensions, obtained from an electron microscopy image (Fig. 5.3) of a SMART "strut V" by Pelton , are listed in Tab. 5.1. In Fig. 5.4 instead the scheme realization is shown even if, as we have said above, we'll stop to the ring realization step.
The input file created by pyFormex was then imported in ABAQUS in order to study where the crack could be collocated and when it could propagate.
Nitinol material, indeed, is implemented in ABAQUS used the user-defined material UMAT ABAQUS subroutine (see Appendix B).

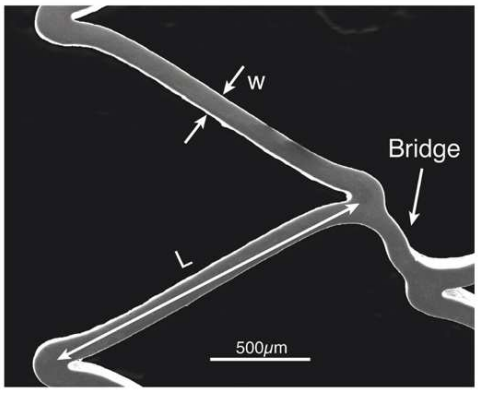

Fig. 5.3: Strut length (L) and width (w) obtained from a microscopy image. The stent wall thickness (th) is projected into the page.

SMART ring dimension	
strut width, w	120 μm
wall thickness, th	200 μm
strut length, L	2 mm
"strut V" number, nV	18
diameter, D	9 mm

Tab. 5.1: SMART ring dimension obtained from scanning electron microscopy image.

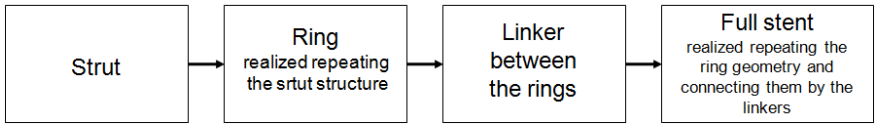

Fig. 5.4: Steps to create stent geometry by pyFormex.

After this introduction, the crack propagation can be studied but, before to do this, it seems appropriate to describe how the components were defined.
We have already discuss about the stent geometry realization so, in the following sections we'll discuss only about the expander, the crimper and the artery realization.

5.2 ABAQUS model realization

The first step illustrated in Fig. 5.2 is the cold expansion from the laser cutted configuration.
The expansion is simulated as a radial displacement applied to a 3D deformable surface without structural properties inserted with a penalty[3] contact into the laser-cutted stent Fig. 5.5. The surface is meshed with 3D, 4-node surface elements with reduced integration

[3]**Penalty contact:** stiff approximation of hard contact. Used by default for finite-sliding, surface-to-surface contact pairs if an hard pressure-overclosure relationship is in effect.

(SFM3D4R), i.e. with elements defined just like membrane elements with zero thickness [65].

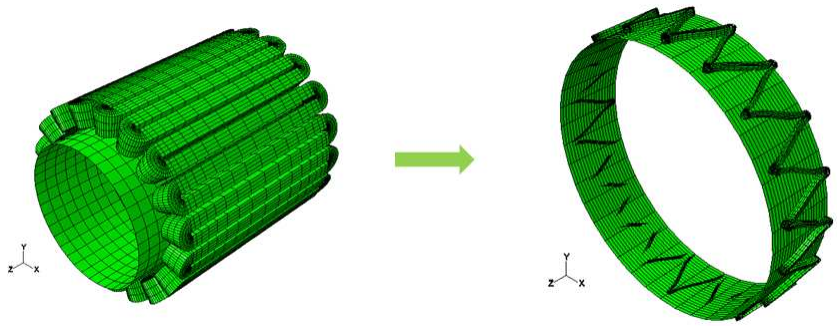

Fig. 5.5: Cold espansion from a laser-cutted configuration to the 9mm nominal diameter.

After the stent is cold expanded to its nominal diameter (9mm), we simulate the crimping into the catheter and the deployment into the artery.
For simplicity, even the catheter (or crimper) is defined as a 3D deformable surface meshed with SFM3D4R elements. Its initial diameter is setted slightly higher than that of the ring and the crimping is simulated applying a radial displacement to its outer surface. When the crimper has touched the ring, the same penalty contact used for the cold-espansion step is used and the ring is so completely compressed (Fig. 5.6).

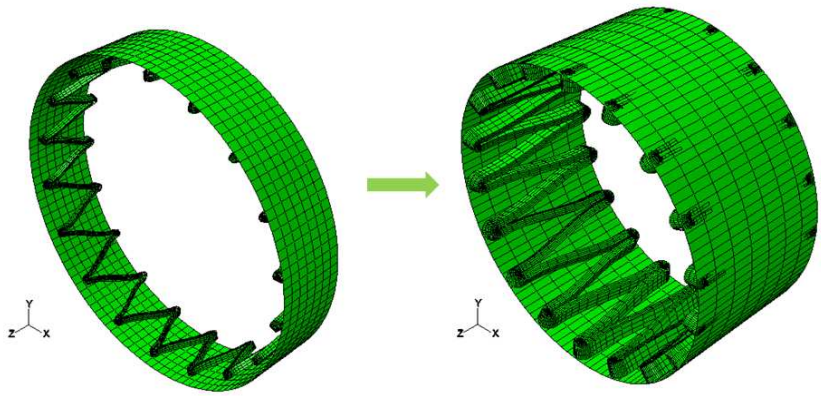

Fig. 5.6: Crimping of the ring applying a radial displacement on the outer surface of this part.

The next step consists of the deployment of the ring in the SFA. The artery was realized

as a cylinder with hyperelastic material and 8-node linear brick, hybrid, constant pressure elements (C3D8RH) [65].
From literature, to have a good simulation, as the ring diameter is 9mm, the SFA diameter should be between 7 and 9 mm and the thickness less or equal to the unity [76, 77].
In Fig. 5.7 we can see the mesh of the vessel with a diameter and a thickness equal to 7mm and 0.7mm.
The deployment into the artery is done deactivating the ring-crimper contact and when the vessel is subjected to systolic pressure (p=0.013 Mpa). Then, diastolic (p=0.010MPa) and yet the systolic pressure should be apply [78].

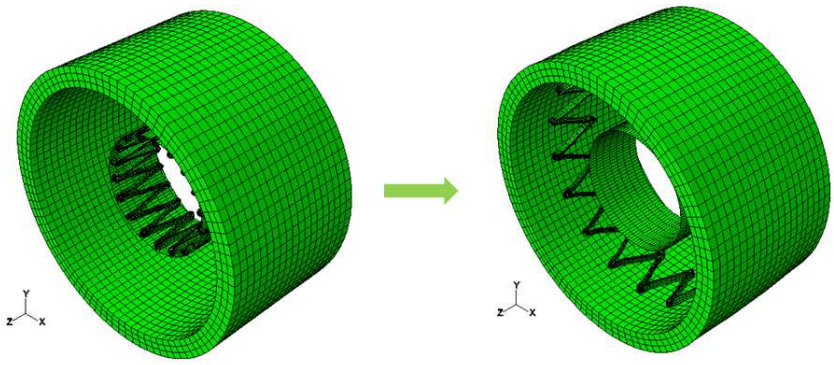

Fig. 5.7: Release of the ring into the pressurized femoral artery.

Now, we are ready to study the crack propagation problem.

5.3 Crack propagation study in a stent ring

The section is organized as follows:

- considerations on which is the best method to simulate the fatigue behavior of a Nitinol stent (stress or strain approach) and determination of peak local stresses/strains;
- crack collocation and application of the VCCT ABAQUS fracture criterion;
- results discussion.

5.3.1 Stress or strain-based fatigue analysis

As discussed in Chapter 3 material fatigue can be evaluated taking into account stresses or strains. In presence of microscopic surface flaws, such as surface imperfections, or cracks creating stress concentrations that can cause the beginning of fatigue crack nucleation, a stress-based analysis is preferred. More precisely, when the flaw size is equal to, or greater than, a critical flaw length (a_c), to quantify fatigue and fracture behavior, stress-based mechanics must be used. When, instead, the size is smaller, the contribution of the stress concentrations is minimal and the nucleation of the cracks is dominated by the cumulative damage of the intrinsic material. In this case both stress- or strain-based criterion can be use [72].

Pelton and his co-workers, in their study on "Fatigue and Durability of Nitinol stents", say that to evaluate the fatigue behavior of Nitinol stents, the strain-based criterion is more appropriate for four mainly reasons:

1. superelastic nitinol stress-strain curve exhibits two distinct elastic regions (Fig. 5.8): the first during the initial crimping up to a critical stress and the second during the subsequently deploying. So, there are non-unique stress values and testing in strain control seems more appropriate;

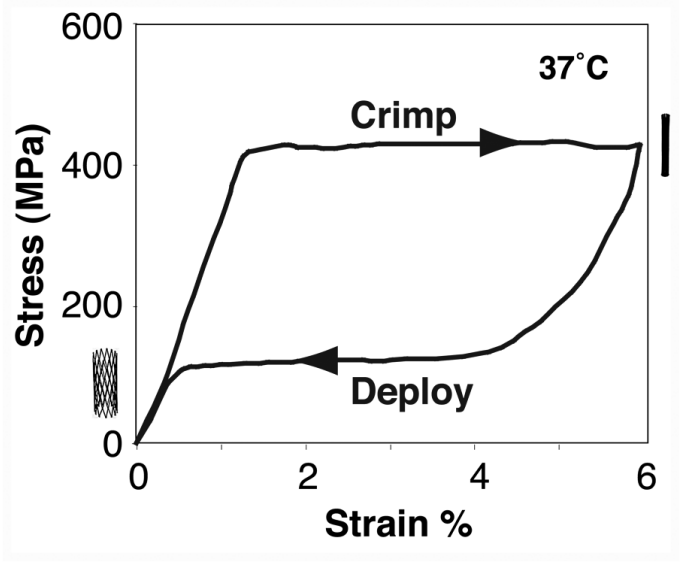

Fig. 5.8: Stress-strain curve of a radial crimp-deploy process.

2. non-pulsatile conditions in peripheral arteries are characterized by changes in length or angle (Section 2.4) and these changes result well aligned with a strain-controlled fatigue analysis [33];

3. do to the anisotropic mechanical response, stent materials, such as Nitinol, have grains that can act as flaws and become sites of crack nucleation [72]. In this case, in presence of microscopic flaws, to quantify the fatigue and fracture behavior, a stress-based analysis must be use. Compared to the critical flaw size (15-50μm), however, nitinol grain size (approximately 100nm) is two orders of magnitude smaller and, therefore, the stress-concentrations effects resulting from the grain size are negligible [73];

4. usually, fracture mechanics may be applied to study unstable crack growth and not what happens between long-crack formation and the subsequent growth. In Nitinol, however, once a crack is nucleated, there is a minimal time between long-crack formation and its growth. The crack so may be considered unstable and fracture mechanics would be applicable [74].

For all these reasons, to identify which are the most likely areas where a crack could be located, we have analyzed with ABAQUS 6.8 the strain of the SMART ring also evaluating if the highest concentration zones change changing the number of "V strut".
Furthermore, as the stent deforms more during the crimping stage, we have evaluated the strain distribution after this step.
In Fig. 5.9 we can see the strain distribution in a crimped SMART ring geometry with several strut number.

From the experimental data obtained by Pelton and his co-workers, it's also possible to resume that:

- as we have seen in Section 3.1.3 the magnitude of the mean strain, in Nitinol, does not limit the fatigue life and the main contribute to fatigue behavior comes from the oscillating strain amplitude (Fig. 5.10);

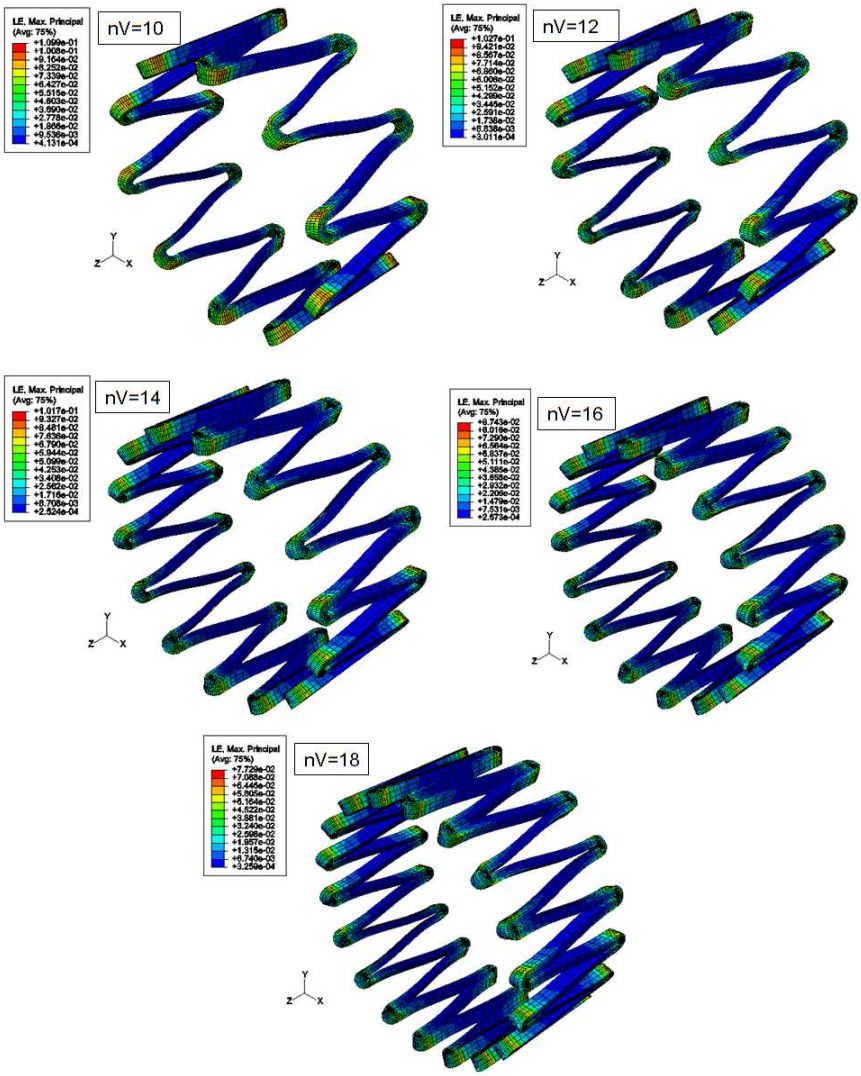

Fig. 5.9: Strain distribution map in a crimped ring with 10, 12, 14, 16 and 18 struts (Vs) to evaluate where the highest strains are concentrated.

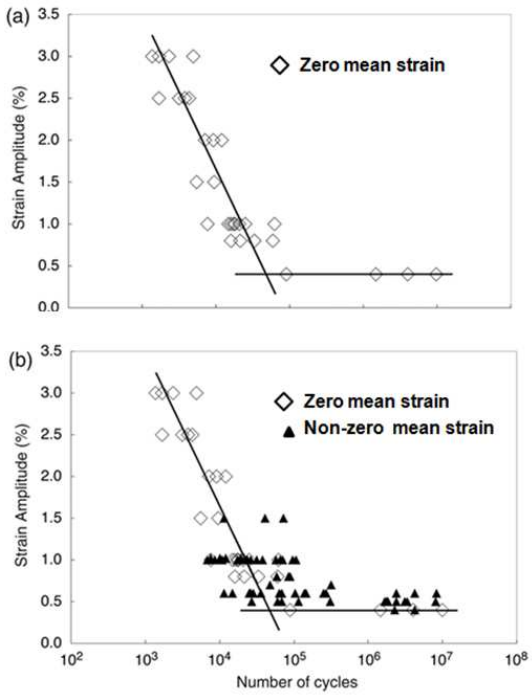

Fig. 5.10: a) Conditions that led to fracture for zero-mean strain. b) Non-zero mean strain data superimposed on the zero-mean data [58].

- the fatigue limit[4] for zero-mean condition and for one million cycles[5] is of about ±0.4% (Fig. 5.11);

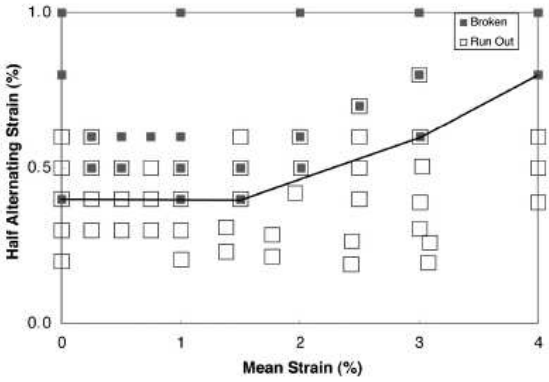

Fig. 5.11: Constant life diagram. Conditions of mean strain and strain amplitude that led to fracture are plotted. Open squares are for conditions that survived the 10^7 cycle test whereas closed squares are for cyclic conditions that led to fracture in less than 10^7 cycles. Note how fatigue limit increases if mean strain increases [58].

These considerations allow us to analyze where a flaw probably nucleates. In Fig. 5.12 , the red areas correspond to those areas where strains are greater than the fatigue limit (ε_e). They are shown for the different number of struts to evaluate if, increasing this number, their size changes. In Fig. 5.13 we can also quantify with which trend the areas change. We can observe that the ring with 18 struts is that with the smaller critical zone and consequently results the most safety case among those showed.

Another evaluation of the critical area can be done regarding the oversizing[6] effect. From Fig. 5.14 it can be note that, if the oversizing effect increases, also the critical area increases.

[4]**Fatigue (or endurance) limit:** lowest strain amplitude where fractures are observed.

[5]According to ASTM recommendations [75] fatigue tests must be conducted at 30Hz until the stents fractured or 10 million cycles is achieved.

[6]**Oversizing:** difference between the stent diameter and the vessel inner diameter.

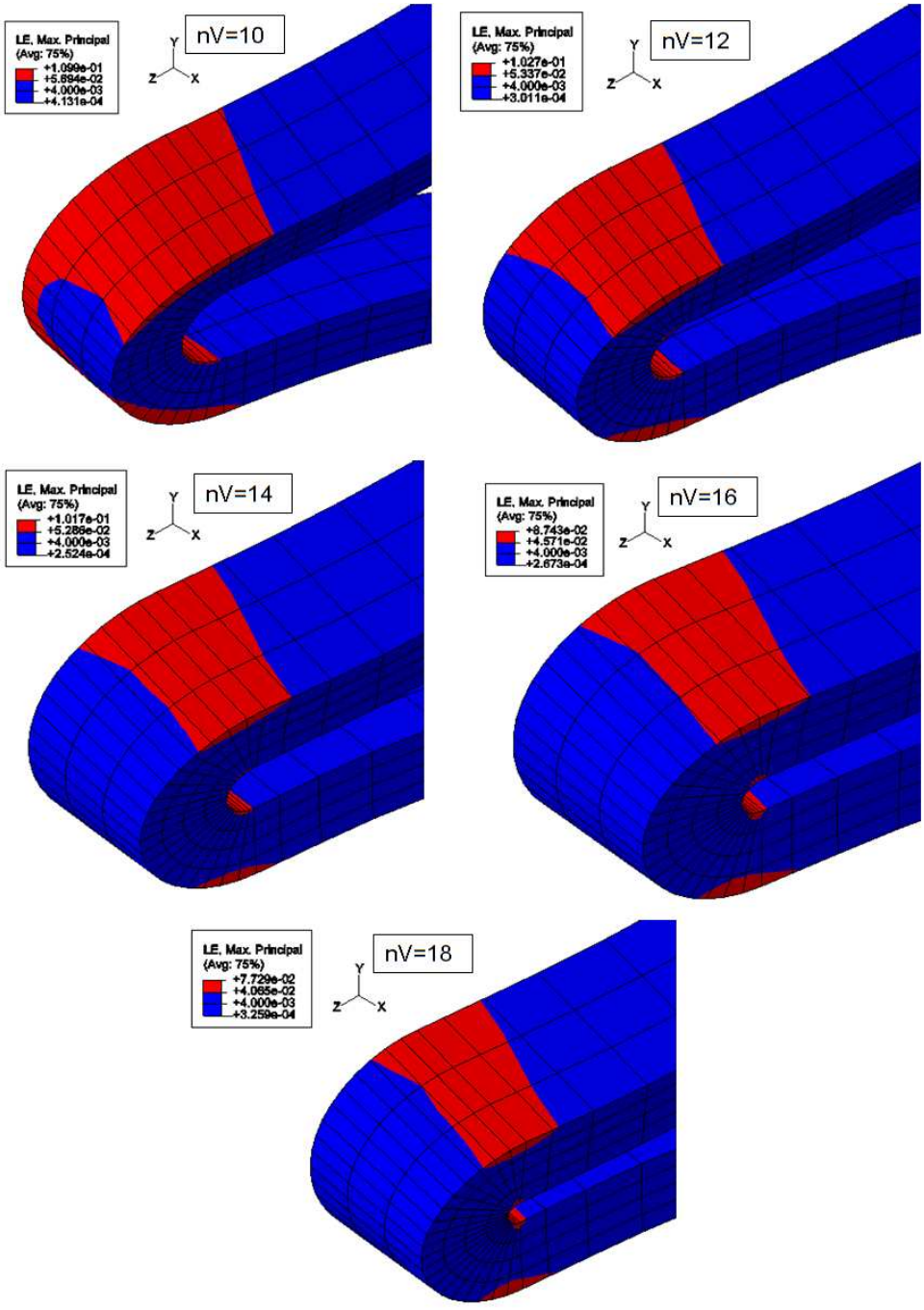

Fig. 5.12: In red the critical areas, i.e. the area where $\varepsilon > 0.4\%$, for different number of struts.

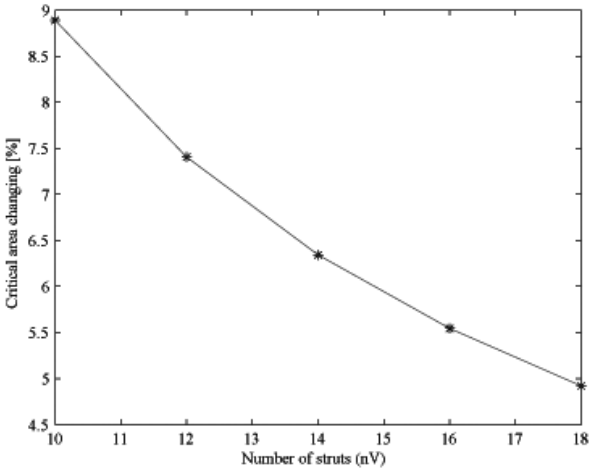

Fig. 5.13: Change of the percentual number of nodes if the number of struts changes. The critical area is defined as the number of nodes where strains are over ε_e normalized by nV.

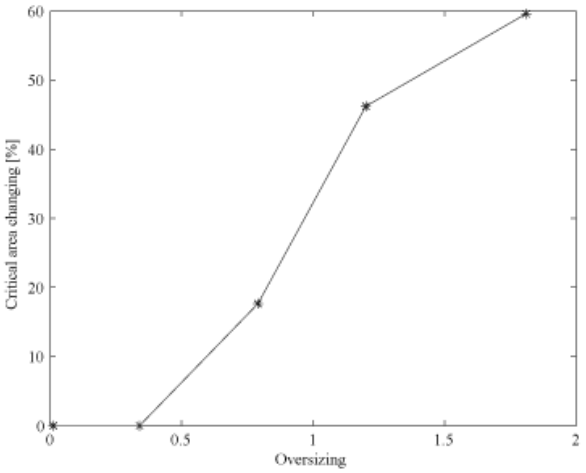

Fig. 5.14: Critical area evaluation if the diameter difference between the ring and the vessel changes. Critical area is defined as the number of the nodes where strains are over the fatigue limit, divided the total number of the nodes of the ring.Note that the critical area increases with the increase of this difference.

5.3.2 Crack collocation and VCCT fracture criterion application

After having established which are the critical zones, the crack is collocated where the value of the max principal strains is greatest, with reference to the previous Fig. 5.9 and Fig. 5.12.

To collocate the crack and apply then the fracture criterion however it was necessary to modify the geometry realized with pyFormex in a way that schematically is explained in Fig. 5.15 and that consists in:

- selection, in the whole ring, of the elements that will be used to define the master and the slave surfaces;
- exportation of the geometry with these elements sets to pyFormex and creation of three separate parts:
  - master part;
  - slave part;
  - ring without the other two parts;
- input file creation and importation in ABAQUS;
- nodes to debond selection and input file change to insert the VCCT criterion.

As we have seen in Chapter 4, to make a crack propagation analysis, the following things must be defined:

- master and slave surfaces, and the node set that identify the initially bonded part;
- initial conditions in order to have that the two surfaces are initially tied and cannot separate;
- fracture criterion to activate the crack propagation capability.

In the previous chapter we have already discuss about the two surfaces and the node set definition; here we'll analyze more in detail the initial condition and the criterion definition.

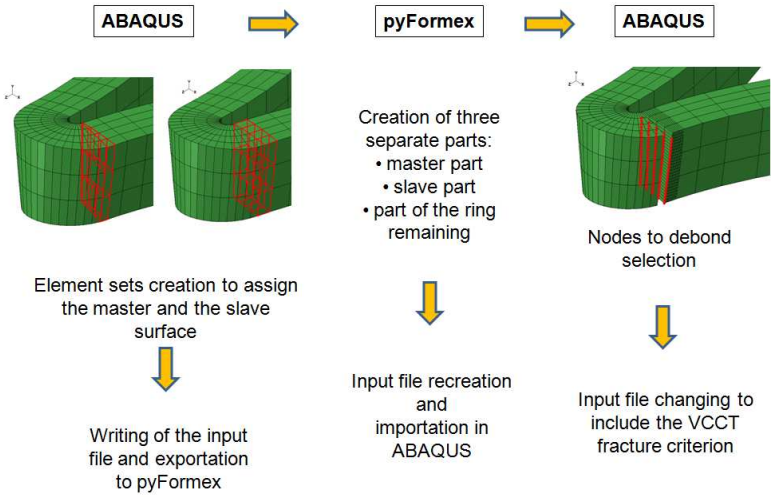

(a)

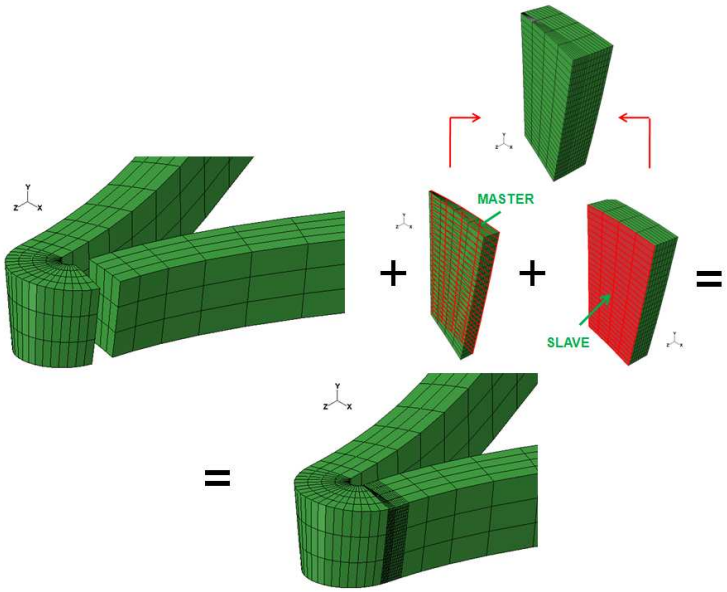

(b)

Fig. 5.15: a) Scheme of the cracked ring creation with the combination of ABAQUS and pyFormex. b) Combination of the three parts with ABAQUS.

As for the initial condition, an hard contact must be defined changing the input file with the following keywords:

```
*INITIAL CONDITIONS,TYPE=CONTACT
slave surf,master surf,node to debond
*Contact Pair,interaction=IntProp-2,small sliding,
type=NODE TO SURFACE
slave surf,master surf
```

where:

- `IntProp-2` defines the interaction type between the master and the slave surfaces (HARD contact);
- `small sliding` assumes that, for geometrically nonlinear analyses, the surfaces may undergo arbitrarily large rotations but a slave node will interact with the same local area of the master surface throughout the analysis;
- `type` defines if the contact is between the two surfaces or between one surface and the nodes of the other surface.

To have the propagation, anyway, also the debonding of the nodes on the slave surface must be defined. This debonding occurs when the fracture criterion specified is satisfied. The lines included in the input file are the following:

```
*debond, slave=slave surf, master=master surf
*FRACTURE CRITERION,TOLERANCE=0.4,TYPE=VCCT,MIXED MODE BEHAVIOR=BK
```

G_{Ic}, G_{IIc}, G_{IIIc}, η

The criterion is applied during the diastolic and systolic pressure application to the vessel as fracture usually occurs after repeated pulse pressure cycles.
From Section 4.3.1 we should remember that G_{Ic} , G_{IIc} , G_{IIIc} and η depend on the material type and for Nitinol they can be deduced from a study of Robertson and Ritchie

(R&R) [72]. R&R characterized, in fact, the fracture toughness (K_{Ic}) behavior of a thin-walled superelastic nitinol tube used to realize a stent. From this value, G_c can be calculated using Eq. 3.3.

In particular, to evaluate how much Nitinol biomedical devices are susceptible to fracture and which are the value of the pertinent engineering parameters (K_{Ic} and fatigue crack growth behavior), they used a compact tension (CT) specimen of a material that accurately followed the forms used for devices (tube) maintaining, however, standard fracture mechanics geometries. Furthermore, as different type of stent fractures and failures are possible, the fracture toughness of the flattened Nitinol tube was evaluated at various angles to the tube drawing direction: longitudinal, circumferential and at 45° (Fig. 5.16).

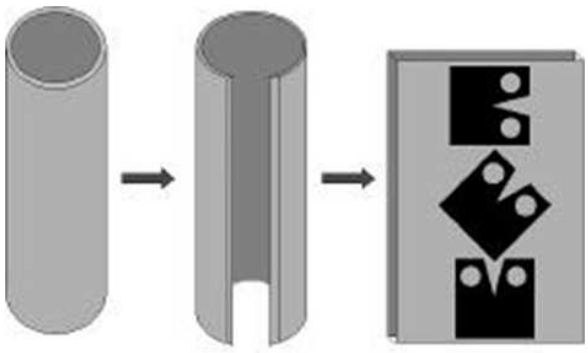

Fig. 5.16: The tube is firstly longitudinally laser cutted, unrolled through a series of shape-setting procedures, and then laser machined to have the C(T) specimens from the flattened configuration in a variety of angles to the drawing direction.

It is found, however, that circumferential crack type causes the predominantly fatigue and overload fracture (Fig. 5.17) so, in our simulation, we'll consider this one. They even say that when plane-strain conditions are not applicable, such as for the stent, toughness values may become both crack size and geometry dependent achieving so elevated values and the measure of toughness K_c results more appropriate than the K_{Ic} value.

Results obtained for all the three sample configurations are shown in Fig. 5.18 and display the stress intensity to initiate crack extension.

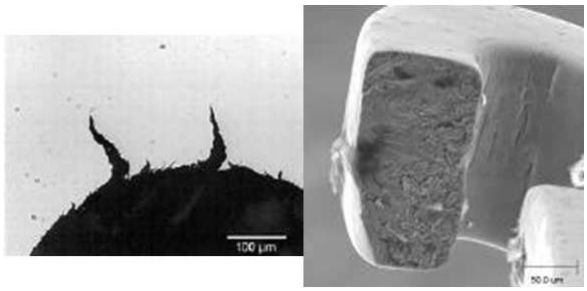

Fig. 5.17: Overload fracture example of a stent. Figure taken by scanning electron microscopy technique [53].

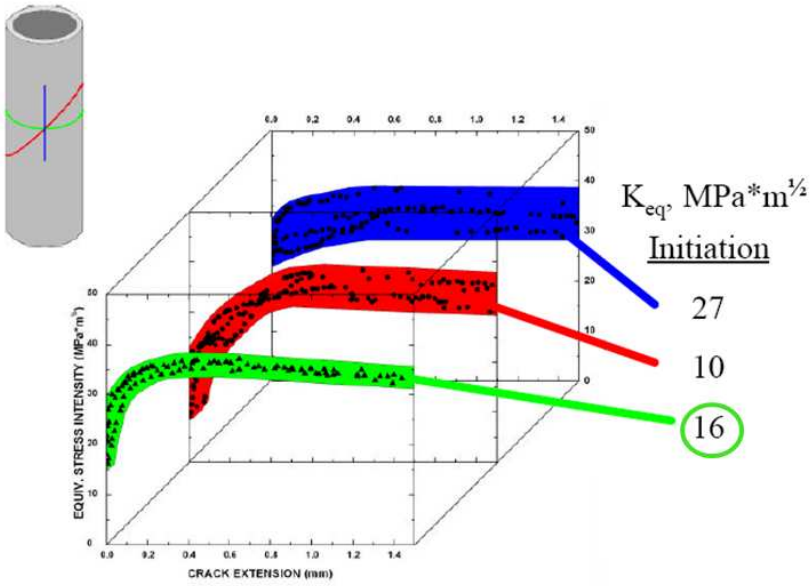

Fig. 5.18: Fracture toughness properties of flattened Nitinol thin-walled tubing (longitudinal, 45° and circumferential orientations). Note the dependence on both crack-growth direction and the extension of a non-stationary crack. Initial pre-notch orientations are given on the tube schematic to the left.

As we have seen previously, we consider the circumferential direction propagation and thus $K_c = 16MPa\sqrt{m}$. Hence:

$$G_c = \frac{K_c^2}{E} = 6.4\,[MPa \cdot mm]$$

where E is the martensite nitinol Young's module (∼40000 Mpa).
Note that we have G_c, but not G_{Ic}, G_{IIc} and G_{IIIc} and that we have no reference for the value of η. In the criterion, however, we must have each of these three values so we should impose them in order to have G_{equivC} equal to 6.4 MPa·mm.

Firstly we have thus done a full analysis (crimping, deployment in the vessel, diastolic and systolic pressure application) with random values of G_{Ic}, G_{IIc}, G_{IIIc} and η; then, from the output we have read G_I, G_{II} and G_{III} values on the nodes along the crack line and we have observed that, with reference to Eq. 4.2,

$$\left(\frac{G_{II} + G_{III}}{G_I + G_{II} + G_{III}}\right)^{\eta} \approx 0$$

So, we have decided to set η to the random value inserted (1.75) and, as the greatest contribution is given by G_I, to set G_{Ic} to 6.4 and G_{IIc} and G_{IIIc} to 6.400000125.Hence we have even that:

$$(G_{IIc} - G_{Ic}) \approx 0$$

Below we can see the complete definition of the criterion.

```
*debond, slave=slave surf, master=master surf
*FRACTURE CRITERION,TOLERANCE=0.4,TYPE=VCCT,MIXED MODE BEHAVIOR=BK
6.4, 6.400000125, 6.400000125, 1.75
```

5.4 Results

From the simulations done, with a straight vessel and a crack initial size of $\approx 16\mu$m, the criterion is not satisfied and the crack does not propagate. In fact:

- $G_{equivC} = 6.4$ MPa·mm;
- $G_{equiv} = \sqrt{G_I^2 + G_{II}^2 + G_{III}^2} \approx 10^{-2}$ in the worst case.

Hence:

$$G_{equiv} < G_{equivC}$$

and the crack propagation cannot occur.

It's possible, however, to establish which are the most affected Modes of fracture (Section 3.2.1) and where they give the highest contribution. In Fig. 5.19 we can see how the strain energy components (G_I, G_{II} and G_{III}) evolve in time for each point of the crack line.
We can note that G_I is greater for the node 1007, G_{II} for the node 1027 and G_{III} for the node 1023, but if we compare the order of magnitude of the highest value of the three components, G_I is the most important, meaning that the ring, under this loading conditions, is more subjected to Mode I type of fracture (Fig. 5.20).

Even a crack of $\approx 50\mu$m is considered. From Fig. 5.21 and Fig. 5.22 we can note that, as for the $\approx 16\mu$m the crack propagation does not occur and Mode I prevails. We can even note that G_I, G_{II} and G_{III} values have increased, showing that we are in a most critical case. In Fig. 5.23, in particular, we can see how much G_I values are different for the two cases illustrated and that for this new case G_I is greater than in the previous one.

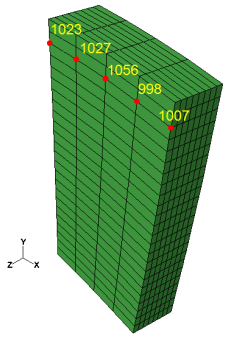

(a)

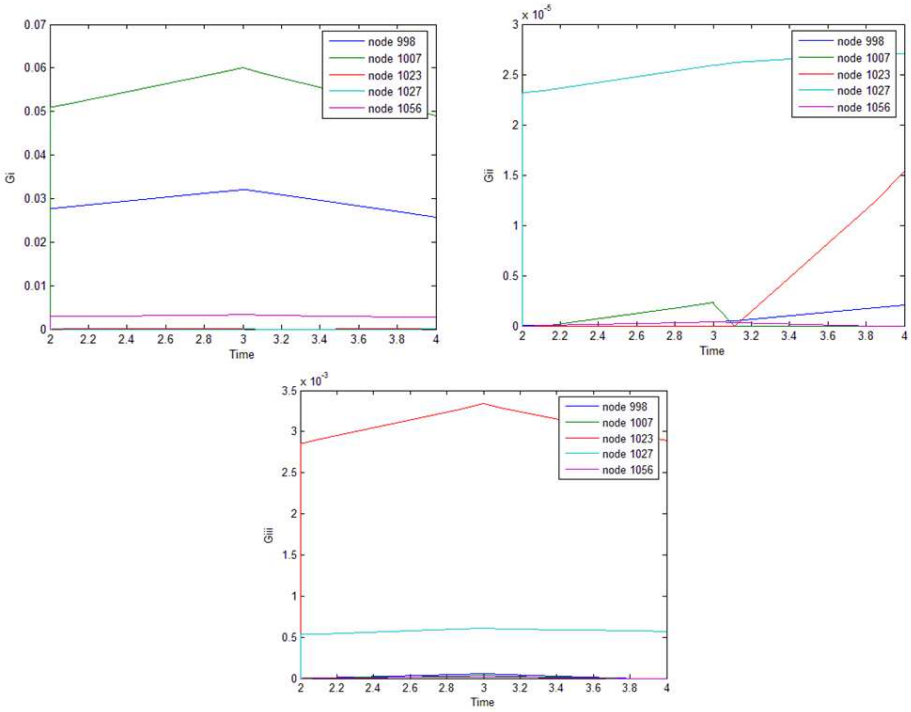

(b)

Fig. 5.19: a) Point nodes on the 16μm crack line. b) G_I, G_{II} and G_{III} evolution for every nodes of the crack line. The time axis starts from 2 because the strain energy is evaluated in the third and in the fourth steps, when diastolic and then systolic pressure are applied. Step-1 and Step-2, instead, are for the crimping and deployment into the vessel.

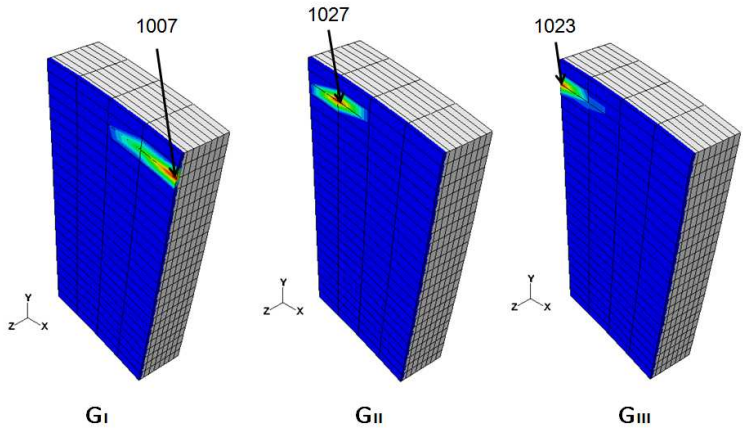

(a)

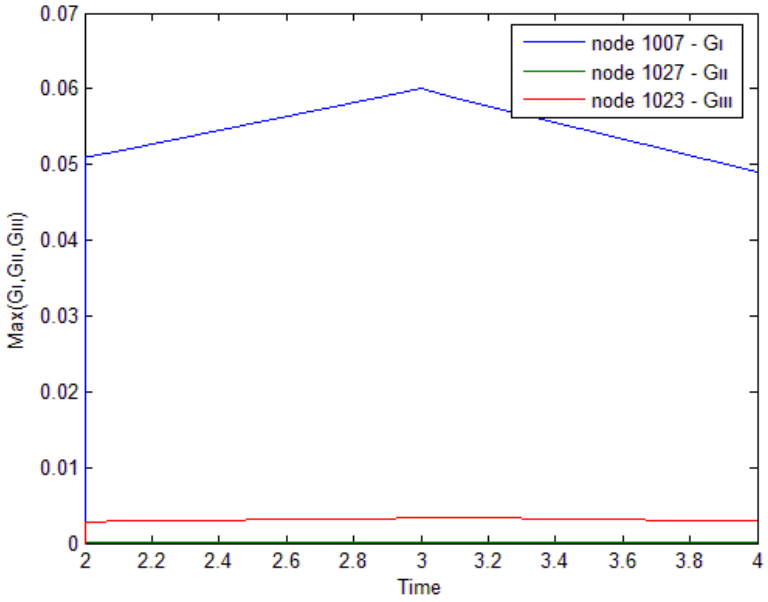

(b)

Fig. 5.20: a) Nodes where G components are greatest. b) Comparison between the highest value of each component of the strain energy to show which is the fracture mode that gives the major contribute.

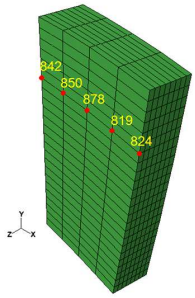

(a)

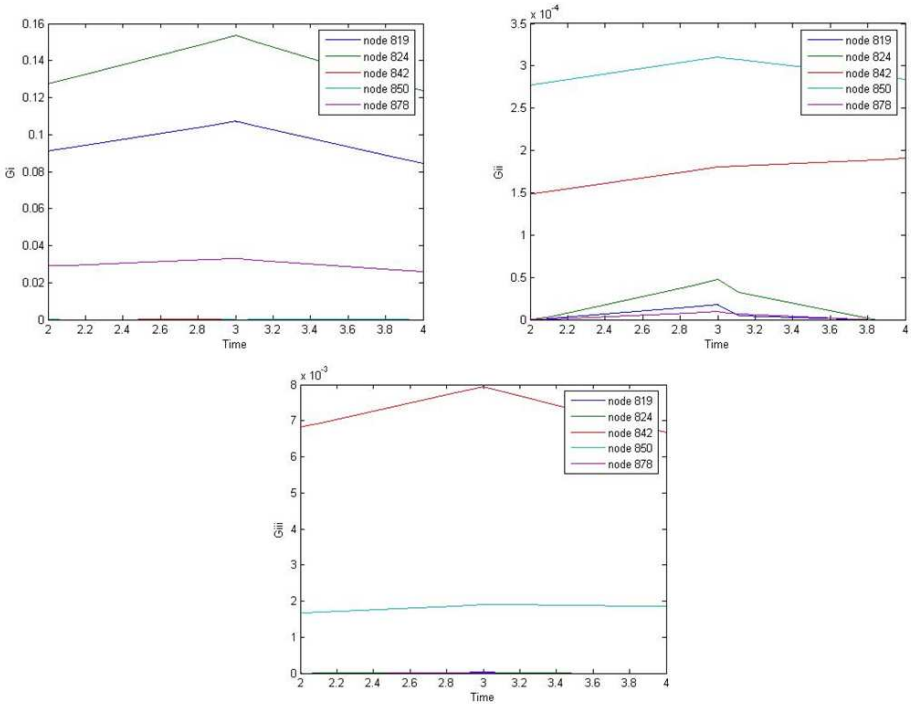

(b)

Fig. 5.21: a) Point nodes on the crack line (size 50μm). b) G_I, G_{II} and G_{III} evolution for every nodes of the crack line.

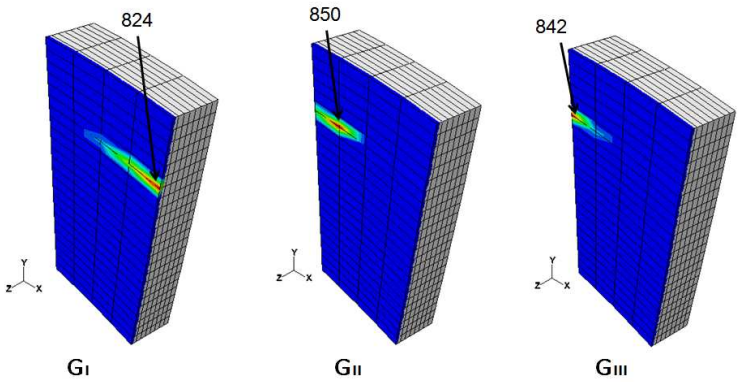

(a)

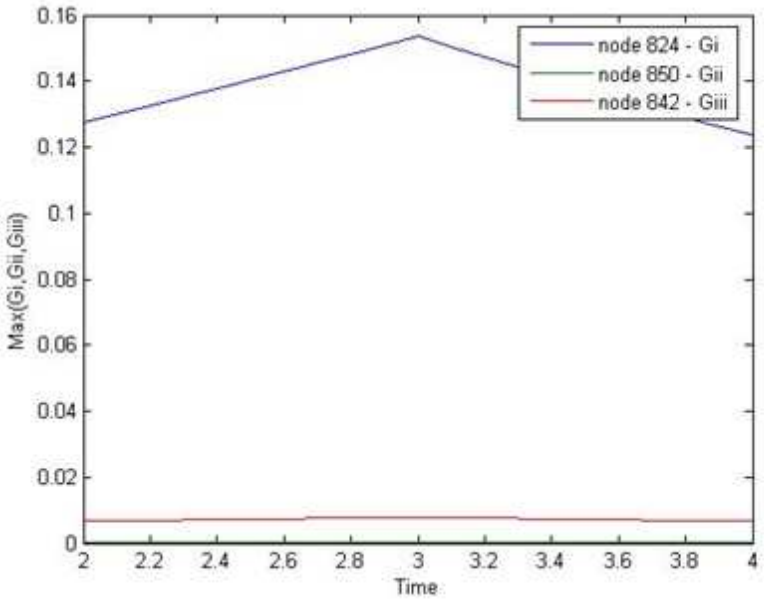

(b)

Fig. 5.22: a) Nodes where G components are greatest. b) Comparison between the highest value of each component of the strain energy to show, also in this case, which is the fracture mode that gives the major contribute. We can note that in both of the cases, G_I, and so Mode I, prevails.

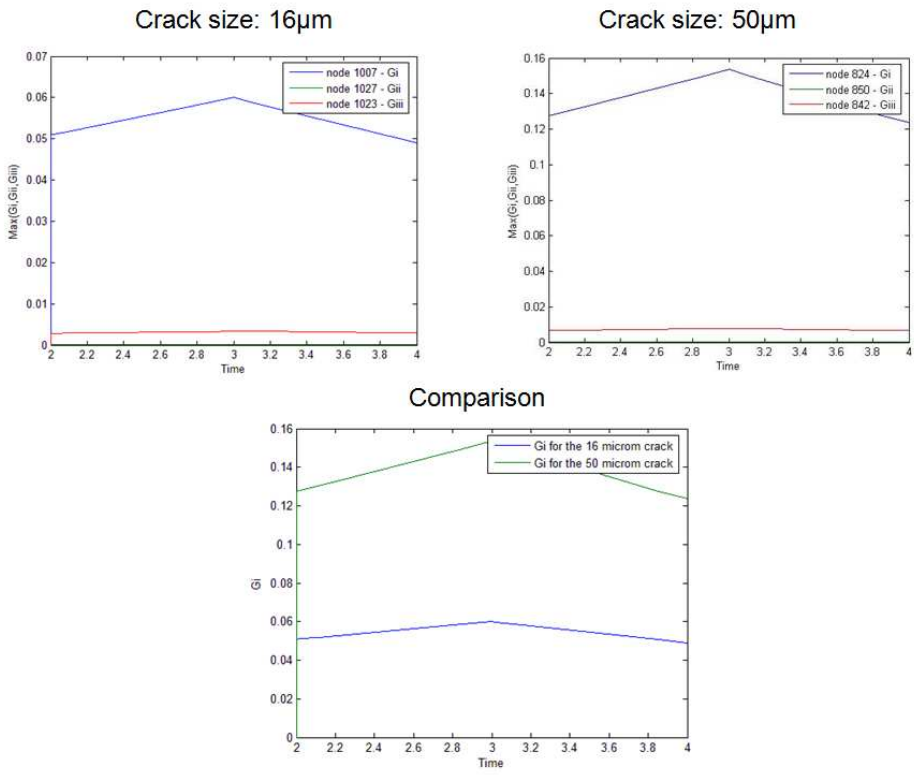

Fig. 5.23: Comparison between Mode I contribution of the two different size cracks($\approx 16\mu$ and $\approx 50\mu$).

Chapter 6

Conclusions and further scenarios

We have presented a possible methodology to study the propagation of a crack in a self-expanding Nitinol stent for the treatment of the superficial femoral artery: SMART stent by Cordis.

We have simulated the main steps of the stent manufacturing and implantation process: cold-espansion, crimping and release into the artery.
Stent geometry was realized by pyFormex, a tool for generating, manipulating and transforming large geometrical models of 3D structures by sequences of mathematical transformations while the simulations of its behavior were performed with ABAQUS 6.8, a finite element commercial software.
Firstly, we have identify a critical region, i.e. the region where a crack could be. Then we have collocated the crack and studied it with an ABAQUS fracture criterion (VCCT) evaluating if it propagates and which are the fracture Modes more responsible in the propagation process. We have considered two different sizes of the crack (16μm and 50μm). Result obtained showed that in both case the crack does not propagate and Mode I is the open crack mode that prevails. Moreover, with a crack of $\approx 50\mu$m we note that we have a more critical condition even if the fracture does not occur.

The methodology proposed however has some important limitations.

In fact we have considered:

- only one ring and not the full stent;
- a straight and healthy artery;
- the pulse pressure but not the biomechanical forces exercised on it.

Moreover:

- we did not have enough data from literature to accurately define the criterion parameters for the Nitinol;
- the criterion is usually used for composite materials;
- the definition of the propagation path is not the realistic one but represents a good approximation.

So in the future it will be interesting to verify if the methodology illustrated is still valid without these limitations and if there are more specific programs to study this type of problems.

Appendix A

Finite Element Analysis: quick review

The appendix want to briefly review what are the basics of the finite element method. [65]
The first step of any finite element simulation is to *discretize* the actual geometry of the structure using just a collection of finite elements where each finite element represents a discrete portion of the physical structure.
The finite elements are joined by shared nodes.
The collection of nodes and finite elements is called the mesh. The number of elements per unit of length, area, or volume in a mesh is referred to the mesh density. In a stress analysis the displacements of the nodes are the fundamental variables that Abaqus calculates. Once the nodal displacements are known, the stresses and strains in each finite element can be determined easily.

A.1 Obtaining nodal displacements using implicit methods

A simple example of a truss, constrained at one end and loaded at the other end as shown in Fig. A.1, is used to introduce some terms and conventions used afterwards.

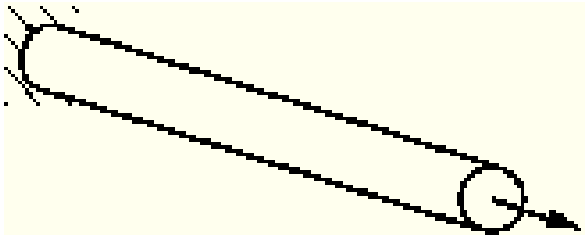

Fig. A.1: Truss problem.

The objective of the analysis is to find the displacement of the free end of the truss, the stress in the truss, and the reaction force at the constrained end of the truss.
In the case showed, a rod (Fig. A.1) will be modeled with two truss elements. In Abaqus truss elements can carry axial loads only. The discretized model is shown in Fig. A.2 together with the node and element labels.

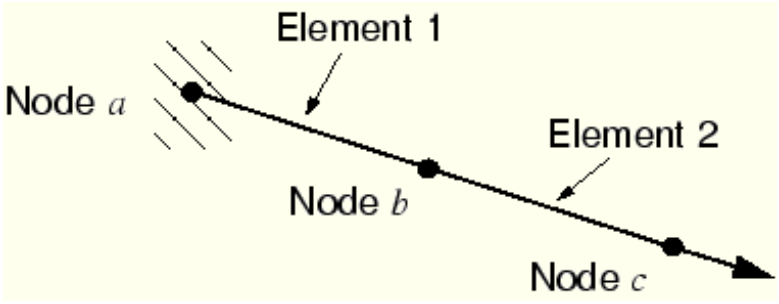

Fig. A.2: Discretized model of the truss problem.

Free-body diagrams for each node in the model are shown in Fig. A.3.
In general each node will carry an external load applied to the model, P, and internal loads, I, caused by stresses in the elements attached to that node. For a model in static equilibrium, the net force acting on each node must be zero; i.e., the internal and external loads at each node must balance each other.

Assuming that the change in length of the rod is small, the strain in element 1 is given by

$$\varepsilon_{11} = \frac{u^b - u^a}{L} \tag{A.1}$$

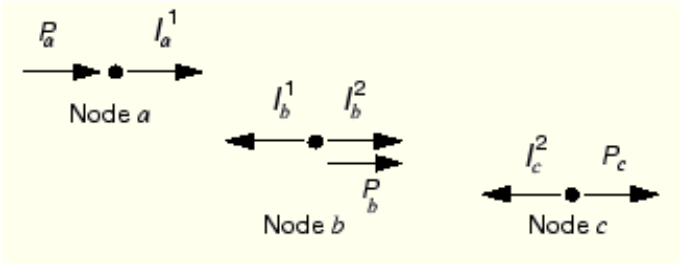

Fig. A.3: Free-body diagram for each node.

where u^a and u^b are the displacements at nodes a and b, respectively, and L is the original length of the element.

Assuming even that the material is elastic, the stress in the rod is given by the strain multiplied by the Young's modulus, E:

$$\sigma_{11} = E\varepsilon_{11} \tag{A.2}$$

The axial force acting on the end node is equivalent to the stress in the rod multiplied by its cross-sectional area, A. Thus, a relationship between internal force, material properties, and displacements is obtained:

$$I_a^1 = \sigma_{11}A = E\varepsilon_{11}A = \frac{EA}{L}\left(u^b - u^a\right) \tag{A.3}$$

Equilibrium at node a can, therefore, be written as

$$P_a + \frac{EA}{L}\left(u^b - u^a\right) = 0 \tag{A.4}$$

Equilibrium at node b must take into account the internal forces acting from both elements joined at that node. The internal force from element 1 is now acting in the opposite direction and so becomes negative. The resulting equation is

$$P_b - \frac{EA}{L}\left(u^b - u^a\right) + \frac{EA}{L}\left(u^c - u^b\right) = 0 \tag{A.5}$$

For node c the equilibrium equation is

$$P_c - \frac{EA}{L}\left(u^c - u^b\right) = 0 \tag{A.6}$$

For implicit methods, the equilibrium equations need to be solved simultaneously to obtain the displacements of all the nodes. This requirement is best achieved by matrix techniques; therefore, write the internal and external force contributions as matrices. If

the properties and dimensions of the two elements are the same, the equilibrium equations can be simplified as follows:

$$\left\{ \begin{array}{c} P_a \\ P_b \\ P_c \end{array} \right\} - \left(\frac{EA}{L} \right) \left[\begin{array}{ccc} 1 & -1 & 0 \\ -1 & 2 & -1 \\ 0 & -1 & 1 \end{array} \right] \left\{ \begin{array}{c} u_a \\ u_b \\ u_c \end{array} \right\} = 0 \tag{A.7}$$

In general, it may be that the element stiffnesses, the EA/L terms, are different from element to element; therefore, write the element stiffnesses as K_1 and K_2 for the two elements in the model. We are interested in obtaining the solution to the equilibrium equation in which the externally applied forces, P, are in equilibrium with the internally generated forces, I. When discussing this equation with reference to convergence and nonlinearity, we write it as

$$\{P\} - \{I\} = 0 \tag{A.8}$$

For the complete two-element, three-node structure we, therefore, modify the signs and rewrite the equilibrium equation as

$$\left\{ \begin{array}{c} P_a \\ P_b \\ P_c \end{array} \right\} - \left[\begin{array}{ccc} K_1 & -K_1 & 0 \\ -K_1 & (K_1 + K_2) & -K_2 \\ 0 & -K_2 & K_2 \end{array} \right] \left\{ \begin{array}{c} u^a \\ u^b \\ u^c \end{array} \right\} = 0 \tag{A.9}$$

In an implicit method, such as that used in Abaqus/Standard, this system of equations can then be solved to obtain values for the three unknown variables: u^b, u^c and P_a(u^a is specified in the problem as 0.0). Once the displacements are known, we can go back and use them to calculate the stresses in the truss elements. Implicit finite element methods require that a system of equations is solved at the end of each solution increment.

The explicit method, in contrast to implicit one and used in Abaqus/Explicit, does not require the solving of a simultaneous system of equations or the calculation of a global stiffness matrix. Instead, the solution is advanced kinematically from one increment to the next.

Appendix B

ABAQUS UMAT subroutine

In this section the subroutine used to characterize nitinol superelasticity with Abaqus/Standard is breafly presented. Its name is UMAT and, in general, it is used to define a material's mechanical behavior.

B.1 UMAT/Nitinol subroutine

As we have see in 3.1 Nitinol's behavior is complex. At rest,the material presents itself in an austenite phase, which behaves linear elastically. Upon loading, this phase transforms into a martensite one, which is also linear elastic even if with different constants than that of the austenite. Upon unloading, the transformation is reversible but the stress levels at which this reversible transformation occurs are smaller than the stresses required to produce the original transformation.

To reproduce all of the features of this material, a user material subroutine (UMAT/Nitinol) was written following the model proposed by Auricchio and Taylor. [80, 81]
The theory decomposes strain into two part the first of which is a purely linear elastic component while the last is a transformation one:

$$\Delta\varepsilon = \Delta\varepsilon^{el} + \Delta\varepsilon^{tr} \tag{B.1}$$

The transformation component, in particular, represents the austenite to martensite transformation that takes place within a range of stress levels that are characteristic of the material.

$$\Delta\varepsilon^{tr} = a\Delta\zeta\frac{\partial F}{\partial\sigma} \tag{B.2}$$

$$F^S \leq F \leq F^F \tag{B.3}$$

where:

- ζ is the fraction of martensite;
- F is a transformation potential.

In particular:

$$\Delta\zeta = f(\sigma,\zeta)\Delta F \tag{B.4}$$

$$F = \bar{\sigma} - ptan\beta + CT \tag{B.5}$$

where:

- $\bar{\sigma}$ is the Mises equivalent stress;
- p is the pressure stress;
- T is the temperature.

B.2 Data for ABAQUS model

The material data required to define superelastic behavior in the ABAQUS model (Fig. B.1) are obtained from straightforward observations of uniaxial tests in terms of loading, unloading, reverse loading and temperature effects.
Specifically:
E_A : Austenite elasticity
ν_A : Austenite Poissons ratio
E_M : Martensite elasticity
ν_M : Martensite Poissons ratio
ε^L : Transformation strain
$\left(\frac{\delta\sigma}{\delta T}\right)_L$: $\delta\sigma/\delta T$ loading

σ_L^S : Start of transformation loading

σ_L^E : End of transformation loading

T_0 : Reference temperature

$\left(\frac{\delta\sigma}{\delta T}\right)_U$: $\delta\sigma/\delta T$ unloading

σ_U^S : Start of transformation unloading

σ_U^E : End of transformation unloading

σ_{CL}^S : Start of transformation stress during loading in compression, as a positive value

ε_V^L : Volumetric transformation strain. If $\varepsilon_V^L = \varepsilon^L$, an associated algorithm is used, with ε_V^L computed based on σ_L^S and σ_{CL}^S

N_A : Number of annealings to be performed during the analysis

N_{S1}-N_{SNA} : Step numbers at which all state dependent variable are set to zero.

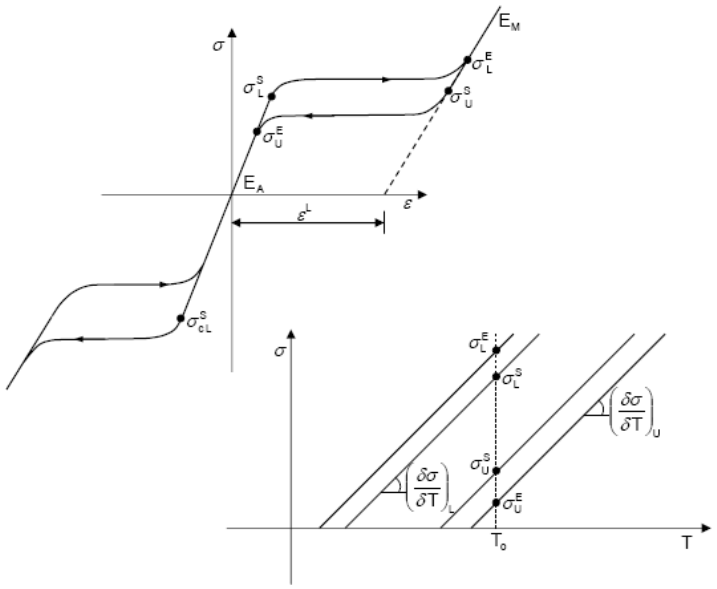

Fig. B.1: Superelastic behavior based on an uniaxial test.

In the ABAQUS input file so, to create the material, we should use these lines:

*MATERIAL, NAME=ABQ_SUPER_ELASTIC_N3D_1

*USER MATERIAL, CONSTANTS= $15 + N_A$

E_A, ν_A, E_M, ν_M, ε^L, $\left(\frac{\delta\sigma}{\delta T}\right)_L$, σ_L^S, σ_L^E

T_0, $\left(\frac{\delta\sigma}{\delta T}\right)_U$, σ_U^S, σ_U^E, σ_{CL}^S, ε_V^L, N_A, $N_{S1}...N_{SNA}$
*DEPVAR
24,

The value inserted for our study are obtained from a Pelton work, [82] and are listed in Tab. B.1.

Parameter	Value
E_A	35877 MPa
ν_A	0.33
E_M	24462 MPa
ν_M	0.33
ε^L	0.0555
$\left(\frac{\delta\sigma}{\delta T}\right)_L$	6.7
σ_L^S	489 MPa
σ_L^E	572 MPa
T_0	22° C
$\left(\frac{\delta\sigma}{\delta T}\right)_U$	6.7
σ_U^S	230 MPa
σ_U^E	147 MPa
σ_{CL}^S	-
ε_V^L	-

Tab. B.1: Parameters inserted in ABAQUS subroutine UMAT to define Nitinol used for stent.

Bibliography

[1] Petersen S, Peto V, Rayner M, Leal J, Luengo FR and Gray A. *European cardiovascular disease statistics*. London: British Heart Foundation, 2005.

[2] Novo S. *The patient with intermittent claudication. Everyday Problems in Clinical Cardiology*. 5th edn Bloch Thomsen PE, Clement DL, eds. Excerpta Medica, Amsterdam, 1995; 3-10.

[3] Rosamond W, Flegal K, Friday G, et al, for the American Heart Association Statistics Committee and Stroke Statistics Subcommittee. *Heart disease and stroke statistics-2007 update: A report from the American Heart Association Statistics Committee and Stroke Statistics Subcommittee*. Circulation. 2007; l15: e69-e171.

[4] Spinler SA. *Challenges associated with metabolic syndrome*. Pharmacotherapy. 2006; 26: 209S-217S.

[5] Novo S. *Classification, epidemiology, risk factors, and natural history of peripheral arterial disease*. Diabetes, Obesity and Metabolism 2002; 4 (Suppl. 2): S1-S6.

[6] Dormandy JA, Rutherford RB, Bakal C et al. *Management of peripheral arterial disease (PAD)*. TransAtlantic Inter-Society Consensus (TASC). Int Angiol 2000; 19 (Suppl.1): 1-310.

[7] Norgren L, Hiatt WR, Dormandy JA, Nehler MR, Harris KA, and Fowkes FGR on behalf of the TASC II Working Group. *Inter-Society Consensus for the Management of Peripheral Arterial Disease (TASC II)*. Journal of vascular surgery 2007; S5A-S67A.

[8] Website: emedicine.medscape.com - Chadi Chahin, Staff Physician, Department of Radiology, Aultman Health Foundation/Mercy Medical Center. *Lower-Extremity Atherosclerotic Arterial Disease*. Article, 2007.

[9] Luther M, Lepantalo M, Alback A, Matzke S. *Amputation rates as a measure of vascular surgical results*. Br J Surg 1996; 83: 241-44.

[10] Wolfe JN. *Defining the outcome of critical ischaemia: a one year prospective study*. Br J Surg 1986; 73: 321.

[11] Gruppo di studio dell'ischemia cronica critica degli arti inferiori. *Long-term mortality and its predictors in patients with critical leg ischemia*. Eur J Vasc Endovascular Surg 1997; 14: 91-95.

[12] Ouriel K. *Peripheral arterial disease*. Lancet 2001; 358: 1257-64.

[13] Brewster DC, Darling RC. *Optimal methods of aortoiliac reconstruction*. Surgery 1978; 84: 739-48.

[14] Veith FJ, Gupta SK, Ascer E, et al. *Six-year prospective multicenter randomized comparison of autologous saphenous vein and expanded polytetrafluoroethylene grafts in infrainguinal arterial reconstructions*. J Vasc Surg 1986; 3: 104-14.

[15] Taylor LM Jr, Edwards JM, Porter JM. *Present status of reversed vein bypass grafting: five-year results of modern series*. J Vasc Surgery 1990; 11: 193-206.

[16] Dotter CT, Judkins MP. *Transluminal treatment of arteriosclerotic obstruction: description of a new technique and a preliminary report of its application*. Circulation 1964; 30: 654-70.

[17] Duerig TW and Wholey M. *A comparison of balloon- and self-expanding stents*. Minimally Invasive Therapy and Allied Technologies 2002.

[18] Morton AC, Crossman D, and Gunn J. *The influence of physical stent parameters upon restenosis*. Pathologie Biologie 2004; 52: 196-205.

[19] Flueckiger F, Sternthal H, Klein GE, Aschauer M, Szolar D, and Kleinhappl G. *Strength, elasticity and plasticity of expandable metal stents: in vitro studies with three types of stress*. Journal of Vascular and Interventional Radiology 1994; 5: 745-750.

[20] Schmidt W, Andresen R, Behrens P, and Schmitz KP. *Comparison of mechanical properties of peripheral self-expanding nitinol and balloon-expandable stainless-steel stents.* CIRSE-Barcelona-Spain 2004.

[21] Duerig TW, Tolomeo DE, Wholey M. *An overview of superelastic stent design.* Minimally Invasive Therapy & Allied Technologies 2000; 9(3/4): 235-246.

[22] Website: www.nhlbi.nih.gov - Atherosclerosis. National Heart Lung and Blood Institute, National Institutes of Healt.

[23] Website: www.vascular.co.nz

[24] Do-Dai-Do, Triller J, Walpoth BH, et al. *A comparison study of self-expandable stents vs balloon angioplasty alone in femoropopliteal artery occlusions.* Cardiovasc Intervent Radiol. 1992; 15: 306-312.

[25] Duda SH, Poerner TC, Wiesinger B, et al. *Drug-eluting stents: potential applications for peripheral arterial occlusive disease.* J Vasc Interv Radiol 2003; 14: 291-301.

[26] Fattori R, Piva T. *Drug-eluting stents in vascular intervention.* Lancet 2003; 361: 247-249.

[27] Duda SH, Bosiers M, Lammer J, et al. *Sirolimus-eluting versus bare nitinol stent for obstructive superficial femoral artery disease: the SIROCCO II trial.* J Vasc Interv Radiol 2005; 16: 331-8.

[28] Roeder BA, Grewe DD, Swift RA. *Expandable stent.* WO/2007/062241. PCT/US2006/045503

[29] Mewissen MW. *Nitinol stents in the femoropopliteal arterial segment.* Endovasc Today 2003; 2(4): 29-34.

[30] Jamsen TS, Manninin HI, Jaakola PA, et al. *Long-term outcome of patients with claudication after balloon angioplasty of the femoropopliteal arteries.* Radiology 2002; 225: 345-352.

[31] Smouse HB, Nikanorov A, LaFlash D. *Biomechanical forces in the femoropopliteal arterial segment.* Endovasc Today 2005; 6: 60-6.

[32] Website: http://www.bartleby.com - Gray H. *Anatomy of the Human Body.* 1918.

[33] Cheng CP, Wilson NM, Hallett RL, Herfkens RJ, and Taylor CA. *In vivo mr angiographic quantification of axial and twisting deformations of the superficial femoral artery resulting from maximum hip and knee flexion.* Journal of Biomechanics 2008; 41(2): 383-9.

[34] Nikanorov A, Smouse HB, Osman K, Bialas M, Shrivastava S, and Schwartz LB. *Fracture of self-expanding nitinol stents stressed in vitro under simulated intravascular conditions.* Journal of vascular surgery 2008; 48: 435-40.

[35] Website: http.//www.drmcdougall.com - The McDougall Newsletter: Volume 5 Issue 9.

[36] Goswami A. A new gait parameterization technique by means of cyclogram moments: application to human slope walking. Gait Posture 1998; 8: 15-36.

[37] Website: http//www.vascularweb.org - Angioplasty and Stenting.

[38] Website: http//www.radiologyinfo.org - Angioplasty and vascular stenting.

[39] Website: http// www.heartsite.com - PTCA or Balloon Angioplasty.

[40] Lampmann LEH. *Stenting in the femoral superficial artery: an overview.* European Journal of Radiology 1999; 276: 279-29.

[41] Lugmayr HF, Holzer H, Kastner M, Riedelsberger H, Auterith A. *Treatment of complex arteriosclerotic lesions with nitinol stents in the superficial femoral and popliteal arteries: a midterm follow-up.* Radiology 2002; 222: 37-43.

[42] Schillinger M, Sabeti S, Loewe C, Dick P, Amighi J, Mlekusch W, Schlager O, Cejna M, Lammer J, and Minar E. *Balloon Angioplasty versus Implantation of Nitinol Stents in the Superficial Femoral Artery.* The new england journal of medicine, established in 1812 may 4, 2006; vol. 354 no. 18.

[43] Scheinert D, Scheinert S, Sax J, Piocorwoski C, Braunlich S, Ulrich M, Biamino G, and Schimdt A. *Prevalence and clinical impact of stent fractures after femoropopliteal stenting.* Journal of American College of Cardiology 2005; 45: 312-5.

[44] Allie DE, Hebert CJ, and Walker CM. *Nitinol stent fracture in the SFA.* Endovascular Today, 2004.

[45] Buehler WJ, Wiley RC, inventors. *Nickel-Based Alloys.* USA Patent 1965; 3: 147-851.

[46] Espinos JP, Fernandez A, Gonzalez-Elipe AR. *Oxidation and diffusion processes in nickel-titanium oxide systems*. Surface Science 1993; 295(3): 402-410.

[47] Kujala S, Pajala A, Kallioinen M, Pramila A, Tuukkanen J, Ryhanen J. *Biocompatibility and strength properties of nitinol shape memory alloy suture in rabbit tendon*. Biomaterials 2004 2004/1; 25(2): 353-358.

[48] Ryhanen J. *Biocompatibility of Nitinol*. SMST-2000: The International Conference on Shape Memory and Superelastic Technologies; Pacific Grove, CA-USA 2001-03; 251-259.

[49] Yahia LH. *Shape Memory Implants*. Berlin: Springer, 2000.

[50] Duerig T, Pelton A, Stockel D. *An overview of nitinol medical applications*. Materials Science and Engineering A 1999; 273-275: 149-160.

[51] Yang D. *Shape memory alloy and smart hybrid composites - advanced materials for the 21st Century*. Materials and Design 2000; 21: 503-50.

[52] Auricchio F. *Shape memory alloys: application, micromechanics, macromodelling and numerical simulations*. 1995.

[53] Website: http://www.me.berkeley.edu/ME117

[54] Duda S et al. *Sirolimus-Eluting Stent For the Treatment of Obstructive Superficial Artery Disease*. Circulation 2002; 106: 1505-1509.

[55] Scheinert D et al. *Prevalence and Clinical Impact of Stent Fracture After Femoropopliteal Stenting*. JACC 2005; 45/02: 312-315.

[56] Boudjemline, et al. *New insights in minimally invasive valve replacement: description of a cooperative approach for the off-pump replacement of mitral valves*. EurHeart J 2005; 26: 2013-2017.

[57] Pelton AR, Gong XY, and Duerig TW. *Fatigue testing of diamond shaped specimen*. Proceedings of the International Conference on Shape Memory and Superelastic Technologies (Pacific Grove, California, 2003), 2003.

[58] Pelton AR, Schroeder V, Mitchell MR, Barney M, and Robertson SW. *Fatigue and durability of nitinol stents*. Journal of the Mechanical Behavior of Biomedical Materials 2008; 153-164.

[59] Suresh S. *Fatigue of materials*. Second edition, Cambridge University press 2006; 288-298.

[60] Lemaitre J and Chaboche JL. *Mechanics of solid materials*. Cambridge University press. 1994.

[61] ASM Handbook. *Fatigue and fracture*. Vol. 19.

[62] Carli F. *Elementi di Meccanica della frattura*. Notes, Universitá di Pavia 2007.

[63] Dassault Systemes Simulia Corporation, Providence, RI, USA.

[64] Website: http://pyFormex.berlios.de

[65] ABAQUS Documentation. Version 6.8, Simulia Corporation.

[66] Benzeggagh M, and Kenane M. *Measurement of Mixed-Mode Delamination Fracture Toughness of Unidirectional Glass/Epoxy Composites with Mixed-Mode Bending Apparatus*. Composite Science and Technology 1996; 56: 439.

[67] Wu EM, and Reuter Jr. RC. *Crack Extension in Fiberglass Reinforced Plastics*. T and M Report, University of Illinois, 1965; vol 275.

[68] Reeder J, Kyongchan S, Chunchu PB, and Ambur DR. *Postbuckling and Growth of Delaminations in Composite Plates Subjected to Axial Compression*. 43rd AIAA/ASME/ASCE/AHS/ASC Structures, Structural Dynamics, and Materials Conference, Denver, Colorado, 2002; 1746: 10.

[69] Abaqus Example Problems Manual. Abaqus version 6.8, Simulia Corporation.

[70] Website: http://www.cordis.com

[71] Marrey RV, Burgermeister R, Grishaber RB, and Ritchie RO. *Fatigue and life prediction for cobalt-chromium stents: A fracture mechanics analysis*. Biomaterials 27, 2006.

[72] Robertson SW, Ritchie RO. *In vitro fatigue-crack growth and fracture toughness behavior of thin-walled superelastic nitinol tube for endovascular stents: a basis for defining the effect of crack-like defects*. Biomaterials 28, 2007; 700-709.

[73] Robertson SW, Ritchie RO. *A fracture-mechanics-based approach to fracture control in biomedical devices manufactured from superelastic nitinol tube*. J. Biomed. Mater. Res. Part B: Appl. Biomaterials, 2007.

[74] Shang DG, Yao WX, Wang DJ. *A new approach to the determination of fatigue crack initiation size*. Int. J. Fatigue 1998; 20: 683-687.

[75] F2477-06. Standard test method for in vitro pulsatile durability testing of vascular stents. ASTM International, 2006.

[76] Instructions for Use Cordis S.M.AR.T.^{TM} Nitinol Stent System.

[77] Vaezy S, Martin R, Kaczkowski P, Keilman G, Goldman B, Yaziji H, Carter S, Caps M, and Crum L. *Use of high-intensity focused ultrasound to control bleeding*. J Vasc Surg 1999; 29: 533-42.

[78] Lally C, Dolan F, and Prendergast PJ. *Cardiovascular stent design and vessel stresses: a finite element analysis*. Journal of Biomechanics 2005; 38: 1574-1581.

[79] Robertson SW. *Stent Failures: Investigation, Research, and Fracture Mechanics*. University of California, Berkeley. ME 117 April 4, 2006.

[80] Auricchio F, Taylor RL. *Shape-memory alloys: modeling and numerical simulations of the finite-strain superelastic behavior*. Comp Meth in Appl Mech and Engnrg 1996; 143: 175-194.

[81] Auricchio F, Taylor RL, Lubliner J. *Shape-memory alloys: macromodeling and numerical simulations of the superelastic behavior*. Comp Meth in Appl Mech and Engnrg 1997; 146: 281-312.

[82] Pelton AR, DiCello J, and Miyazaki S. *Self-expanding nitinol stents: material and design considerations*. Minimally Invasive Therapy and Allied Technologies 2000; 9(1): 107-118.